C. R. Physique 17 (2016) 113–139

Contents lists available at ScienceDirect

Comptes Rendus Physique

www.sciencedirect.com

Iron-based superconductors / Supraconducteurs à base de fer

Charge nematicity and electronic Raman scattering in iron-based superconductors

Nématicité de charge et diffusion Raman électronique dans les supraconducteurs au fer

Yann Gallais *, Indranil Paul *

Laboratoire "Matériaux et Phénomènes quantiques", Université Paris-Diderot–Paris-7 & CNRS, UMR 7162, 75205 Paris, France

ARTICLE INFO

Article history:
Available online 10 November 2015

Keywords:
Iron-based superconductors
Raman scattering
Nematicity

Mots-clés :
Supraconducteurs au fer
Diffusion Raman
Nématicité

ABSTRACT

We review the recent developments in electronic Raman scattering measurements of charge nematic fluctuations in iron-based superconductors. A simple theoretical framework of a *d*-wave Pomeranchuk transition is proposed in order to capture the salient features of the spectra. We discuss the available Raman data in the normal state of 122 iron-based systems, particularly Co-doped $BaFe_2As_2$, and we show that the low-energy quasi-elastic peak, the extracted nematic susceptibility and the scattering rates are consistent with an electronic-driven structural phase transition. In the superconducting state with a full gap, the quasi-elastic peak transforms into a finite-frequency nematic resonance, evidences for which are particularly strong in the electron-doped systems. A crucial feature of the analysis is the fact that the electronic Raman signal is unaffected by the acoustic phonons. This makes Raman spectroscopy a unique probe of electronic nematicity.

RÉSUMÉ

Nous présentons dans cette revue les mesures de fluctuations de charge nématiques par diffusion Raman électronique dans les supraconducteurs au fer. A cadre théorique simple d'une transition de Pomeranchuk d'onde *d* est proposé afin comprendre les spectres Raman. Nous discutons ensuite des données Raman publiées dans l'état normal des composés 122, en particulier $BaFe_2As_2$ dopé au Co, et nous montrons que le pic quasi-élastique observé, la susceptibilité nématique extraite et le taux de diffusion sont en accord avec l'idée d'une transition structurale pilotée par les degrés de liberté électroniques. Dans l'état supraconducteur et en l'absence de noeuds dans le gap, le pic quasi-élastique se transforme en une résonance nématique à fréquence finie. La signature expérimentale de cette résonance nématique est particulièrement claire dans le cas des systèmes dopés électron. Un aspect crucial de l'analyse est le fait que la diffusion Raman électronique n'est

* Corresponding authors.
E-mail addresses: yann.gallais@univ-paris-diderot.fr (Y. Gallais), indranil.paul@univ-paris-diderot.fr (I. Paul).

http://dx.doi.org/10.1016/j.crhy.2015.10.001

pas affectée par les phonons acoustiques, faisant de cette technique une sonde unique de la nématicité électronique.

1. Introduction

The study of correlated phases of matter obtained a big boost with the discovery of the iron-based superconductors (Fe SC) in 2008 [1]. These systems are interesting not just because they exhibit superconductivity at temperatures as high as 55 K, but also because they are a rich playground where the lattice and the electronic charge, spin, and orbital degrees of freedom all play important roles. This complex interplay invariably leads to competition between various interesting phases that can be stabilized by varying temperature, by doping carriers, and by applying pressure. Understanding this rich physics is a considerable challenge, and consequently the topic continues to be an active area of research in condensed matter systems [2,3].

Unlike the cuprate high-temperature superconductors where the parent compounds are Mott insulators, the Fe SC systems are multi-band and multi-orbital metals at all doping values. The undoped and the lightly doped compounds undergo a structural transition from a high-temperature ($T > T_S$) tetragonal unit cell to a low-temperature ($T < T_S$) orthorhombic phase (in the case of $Fe_{1+y}Te_{1-x}Se_x$ the low-T phase is monoclinic for small x), which is followed in close proximity in temperature by a magnetic transition at T_N, below which the system is antiferromagnetic. These transitions are suppressed with electron or hole doping, and beyond a certain doping value the system becomes superconducting with an unusually high transition temperature T_C. Initial investigations of the superconductivity and its origin have focused mainly on the interplay between a stripe-like antiferromagnetism (where the magnetic ordering wave-vector is $(\pi, 0)$ or $(0, \pi)$ in the 1Fe/cell notation) and superconductivity. While the issue is not entirely settled, it is popularly believed that the fluctuations associated with the stripe antiferromagnetism give rise to a $s^{\pm}$ superconducting pairing symmetry [4–6] in most, but possibly not all [7], Fe SC families.

Ever since the reports of strongly anisotropic in-plane transport in the 122 systems [8] in the orthorhombic phase, a lot of attention has been given to study the property of nematicity in these materials. A nematic phase of matter is one that breaks rotational symmetry spontaneously, while preserving translational symmetry. Such phases have been studied extensively since the 1970s in classical soft matter systems [9], but relatively less is known about their quantum counterparts in electronic systems. However, their existence has been widely postulated for strongly correlated materials such as quantum Hall systems, cuprates, bilayer ruthenates [10], and most recently in the Fe SC. In the presence of a crystalline lattice, a nematic phase breaks discrete rotational symmetry, and as a consequence the associated order parameter is an Ising variable. In the context of the Fe SC, this order parameter is non-zero in the orthorhombic phase where the C_4 symmetry of the Fe unit cell is broken at the structural transition T_S. Note that, in certain systems, the structural and the magnetic transition are simultaneous ($T_S = T_N$), and, since the magnetic order by itself breaks C_4 symmetry, it is not clear whether the nematicity is a mere by-product of the magnetic order. Consequently, the issue of nematicity is more sharply posed for those systems where the structural transition precedes the magnetic one ($T_S > T_N$), leaving a finite temperature interval where C_4 symmetry is broken while the system remains paramagnetic [11–14]. The extreme example of this trend appears to be FeSe where only a structural transition [15,16] is detected and the system remains paramagnetic down to its SC phase [17,18], hinting that nematic degrees of freedom may not be necessarily linked to magnetic ones.

The microscopic origin of the nematic order is currently not known with certainty. One scenario is that the structural transition is, in fact, an instability driven by the anharmonic lattice potential, in which case the primary order parameter is the lattice orthorhombicity, and the electronic degrees of freedom are secondary order parameters that passively follow the symmetry breaking induced by the lattice strain. A second scenario is that the C_4 symmetry breaking is driven by electronic interactions, in which case the primary order parameter is electronic in origin. Within this picture, one possibility is the spin-nematic transition whereby the spins of the two Fe sublattices phase-lock, which breaks C_4 symmetry, without developing a spontaneous magnetization, i.e., without breaking time reversal symmetry [19–27]. A second possibility is ferro-orbital ordering [28–32], where either the occupations or the hopping matrix elements (or both) of the d_{xz} and the d_{yz} orbitals of Fe become inequivalent. Besides these two scenarios, other possibilities include a d-wave Pomeranchuk instability [33], in which the Fermi surfaces undergo symmetry-breaking distortions due to interaction effects, as well as a valley density wave [34].

On the experimental side, initial studies have focused on the strong anisotropy of the electronic properties in the orthorhombic C_4 symmetry-broken phase. Transport [8,35–39], optical conductivity [40–44], ARPES [45,46], and neutron scattering [47–49] (reviewed in a separate contribution to this issue [50]) performed on mechanically detwinned crystals all reported considerable electronic anisotropies. While it has been argued that the magnitudes of the measured anisotropies are too large to be due to the lattice orthorhombicity (which is 0.4 percent at most), such arguments can be at best quantitative, and therefore they do not convincingly rule out the lattice-driven scenario. Furthermore, even within the electronic-driven scenario, the above experiments cannot uniquely identify whether the primary order parameter is composed of electronic charge, spin or orbital degrees of freedom [51].

One difficulty in interpreting the above experiments is that, in the symmetry-broken phase, all the above order parameters are non-zero, and consequently it is difficult to identify the one which is most relevant. From this point of view, it is desirable to set experiments that measure relevant susceptibilities in the C_4 symmetric phase, and search for signatures of nematic fluctuations that soften upon approaching T_S. One obvious possibility is the measurement of the orthorhombic elastic constant that measures the force constant associated with the orthorhombic strain of the lattice [23,52–54]. Such studies are reviewed in a separate contribution to this issue [55]. However, note that an elastic constant measurement cannot, by itself, clearly distinguish between a lattice-driven from an electronic-driven scenario of nematicity. This is because an elastic constant measurement is a thermodynamic probe, and therefore, once the interaction between electrons with the acoustic phonons is taken into account, in both scenarios one would conclude that there is a softening of the relevant elastic constant. Next, in the spin-nematic scenario, the fluctuations of the order parameter (which is a two-spin operator) involve a four-spin susceptibility. This poses a technical difficulty because, while NMR and neutron scattering can give crucial information on the evolution of the spin fluctuation spectrum [47,56–61] and the spin susceptibility at the antiferromagnetic wave-vector, they cannot easily access the four-spin susceptibility. This means that, at present there is no direct probe to test the fluctuations associated with a spin-nematic order parameter. An alternative way to probe the nematic susceptibility was pioneered by Chu et al. [62–64], who were able to extract the nematic component of the elasto-resistivity tensor in the tetragonal phase. This was achieved by performing strain dependent measurements of the transport anisotropy. Because the method allows a direct extraction of the lattice-free electronic nematic susceptibility, the observed divergence is a strong evidence for an electronic-driven structural phase transition. A drawback, however, is the difficulty to associate the extracted nematic susceptibility with a microscopic nematic order parameter.

On the other hand, in this review we argue that electronic Raman scattering allows a direct access to the fluctuations of the charge nematic order parameter, or equivalently the d-wave Pomeranchuk order parameter. This ability of Raman measurements has been somewhat overlooked in the past, although earlier Raman experiments in underdoped cuprates could possibly be interpreted along these lines [65]. We show in this review that Raman experiments in Fe SC give compelling evidences of the presence of nearly-critical charge nematic fluctuations in the tetragonal phase. These experiments also allow a direct extraction of the associated nematic susceptibility, which contains information about the incipient phase instability involving the *purely electronic* degrees of freedom. This is because the electronic Raman response is a spectroscopic probe, and it is "opaque" to the acoustic phonons in the system. In fact, this property of the electronic Raman response function provides a *qualitative method* to distinguish between lattice-driven versus electronically-driven scenarios of nematicity. It can be shown that in the former case the extracted nematic susceptibility from the Raman data should not show any signature of softening with lowering temperature. The fact that in Fe SC one does see softening *proves conclusively that the nematicity is electron-driven rather than lattice-driven*. This establishes Raman scattering as a key probe of translation symmetry preserving Fermi surface distortions that can be used to investigate other correlated electron systems such as the bilayer ruthenates and the cuprates where this kind of instability has been proposed, but not yet confirmed unequivocally from an experimental point of view.

This review is divided into two main parts, one theoretical and the other experimental. We start with the theory part, which aims at giving a simple framework to understand how Raman scattering can be used to probe the charge nematic susceptibility and its associated dynamical fluctuations in an electron system. The approach is quite general, and the main features are expected to hold for the case of the Fe SC. In Section 2.1, we consider a generic one-band model with a charge nematic or Pomeranchuk instability where the Fermi surface breaks the C_4 symmetry. In Section 2.2, we provide analytical expressions for its critical fluctuations within the random-phase approximation (RPA). In Section 3.1, we show that electronic Raman scattering directly couples with the charge nematic fluctuations, provided the appropriate symmetry channel is probed. In the case of the Fe SC, this is the B_{1g} channel (which transforms as $(x^2 - y^2)$ in the 1Fe/cell notation). We show in Section 3.2 that the presence of these nematic fluctuations leads to the emergence of a quasi-elastic peak whose linewidth tends to vanish at the incipient pure electronic (i.e., one without lattice coupling) nematic phase transition. We further show in Section 3.3 that Raman scattering measurements can access the charge nematic susceptibility, but only in the dynamical limit as opposed to the static limit which is relevant for the definition of the thermodynamic phase transition involving the C_4 symmetry breaking. While these two limits are the same for a pure electronic system, the coupling with the lattice induces a key difference between the two limits making Raman scattering measurement essentially blind to the linear coupling between the electron-nematic variable and the lattice orthorhombic strain. We conclude the theory part by discussing in Section 3.4 some of the additional subtleties associated with the multi-band nature of Fe SC. In particular, we point out the existence of different flavors of charge nematicity when the orbital quantum number is taken into account. However, Raman measurements cannot distinguish between the various charge nematic order parameters that are possible in a multi-orbital environment.

In the experimental part, after reviewing briefly the details of the Raman experiments in Section 4, we discuss the observation of charge nematic fluctuations in the tetragonal phase of electron-doped $Ba(Fe_{1-x}Co_xAs)_2$. In Section 5.1, we focus on the behavior of the extracted charge nematic susceptibility as a function of Co electron doping and temperature. We then compare in Section 5.2 Raman results with two other complementary probes of nematic fluctuations in the tetragonal state, elastoresistivity and elastic constant measurements, and conclude that all three measurement are consistent with an electronic-driven structural phase transition. We briefly comment on the role of disorder in Section 5.3 by comparing Ba122 and Sr122 systems. In Section 6.1, we discuss the finite frequency spectra of the nematic fluctuations and show that it is consistent with expectations from a simple mean-field approach of the nematic phase transition (Section 6.2). We then show

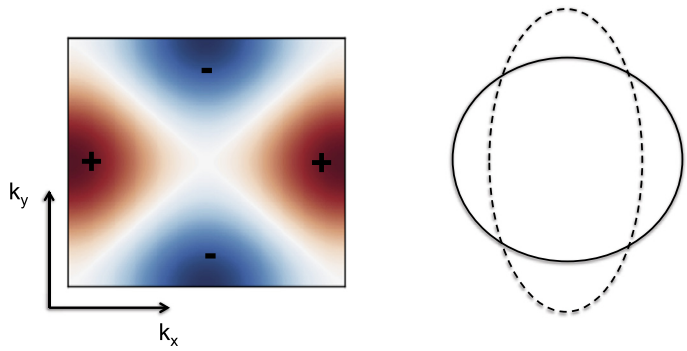

Fig. 1. Left: B_{1g} symmetry form factor h_k of the Pomeranchuk or charge nematic operator in k-space. Right: associated Fermi surface deformation in a one-band model. The original spherical Fermi surface is distorted into an elliptical one in the charge nematic phase.

in Section 6.3 that Raman and shear modulus measurements can be consistently reproduced using a simple Landau-type mean-field picture with a linear coupling between charge and lattice nematicity. We conclude this review by addressing the fate of nematic fluctuations in the superconducting state (Section 7) and show that they can give rise to a novel collective mode, a nematic resonance, near to the nematic quantum critical point. Experiments on electron-doped Fe SC (Co–Ba122 and Co–Na111) appear to support its existence.

2. Theory: charge nematic instability

In this section, we provide a microscopic description of charge nematic instability triggered by a phenomenologically-introduced electron–electron interaction.

2.1. Model

We consider a system of interacting electrons on a square lattice, simultaneously scattered by point-like impurity described by the Hamiltonian

$$\mathcal{H} = \mathcal{H}_0 + \mathcal{H}_I + V \tag{1}$$

In the above

$$\mathcal{H}_0 = \sum_{\mathbf{k},\sigma} \epsilon_{\mathbf{k}} c^\dagger_{\mathbf{k},\sigma} c_{\mathbf{k},\sigma} \tag{2}$$

is the bare Hamiltonian of a band of electrons with dispersion $\epsilon_{\mathbf{k}}$, having lattice momentum $\mathbf{k}$ and spin σ as quantum numbers, and described by usual creation/annihilation operators ($c^\dagger_{\mathbf{k},\sigma}, c_{\mathbf{k},\sigma}$). Note that, while the Fe-based superconductors (Fe SC) are multi-band systems, here, for the sake of simplicity, we restrict ourselves to a one-band model. Our main goal is to discuss certain qualitative physics, rather than quantitative ones, involving Raman spectroscopy near a charge nematic transition. We expect the main conclusions of this analysis to remain unchanged for a multi-band environment. Of course, in a multi-band system there are inter-band transitions that contribute to the Raman response, which are absent in a one-band model. However, typically such inter-band transitions are not related to criticality involving charge nematic transition. The latter is essentially a Fermi surface instability, and consequently, its critical fluctuations involve only intraband excitations. In Section 3.4, we comment about the additional subtleties associated with nematic instabilities in a multi-orbital and multi-band environment.

The interaction between the electrons is described by

$$\mathcal{H}_I = -\frac{g_0}{2} \sum_{\mathbf{q}} O_n(-\mathbf{q}) O_n(\mathbf{q}) \tag{3}$$

The operator

$$O_n(\mathbf{q}) \equiv \frac{1}{\sqrt{\mathcal{N}}} \sum_{\mathbf{k},\sigma} f_{\mathbf{k},\mathbf{q}} c^\dagger_{\mathbf{k}+\mathbf{q},\sigma} c_{\mathbf{k},\sigma} \tag{4}$$

where $f_{\mathbf{k},\mathbf{q}} = (h_{\mathbf{k}} + h_{\mathbf{k}+\mathbf{q}})/2$ with the B_{1g} (or equivalently $x^2 - y^2$) form factor $h_{\mathbf{k}} = \cos k_x - \cos k_y$, is the Fourier transform of the charge nematic operator (see Fig. 1)

$$O_n(\mathbf{r}_i) = \frac{1}{4}\left[\left(c^\dagger_i c_{i-\hat{x}} + c^\dagger_i c_{i+\hat{x}} + \text{h.c.}\right) - \hat{x} \to \hat{y}\right] \tag{5}$$

$\mathbf{r}_i$ is the position of the lattice site i, and $\mathcal{N}$ is the total number of sites. In the high-temperature C_4-symmetric phase, $\langle O_n(\mathbf{r}_i)\rangle = 0$, while in the symmetry-broken phase, $\langle O_n(\mathbf{r}_i)\rangle = \delta_0$, $\forall i$, implying a charge nematic phase that preserves translation symmetry but not the discrete $\pi/2$ rotational symmetry, such that the hopping matrix elements along $\hat{x}$ and $\hat{y}$ are inequivalent. This is the lattice version of a Pomeranchuk transition [10,66] where a spherical (or circular in two dimensions) Fermi surface becomes ellipsoidal (or elliptical), and indeed in the following we do not distinguish between the names "charge nematic" and "Pomeranchuk". We take the constant $g_0 > 0$, implying that C_4 symmetry-breaking distortions of the Fermi surface are energetically favored by the interaction term. This is a pre-requisite for a charge nematic instability, at least in weak coupling theories involving random phase approximation.

Evidently, there is non-trivial physics involved in transforming the usual short-range repulsion between the electrons into an interaction given by Eq. (3), and in the Fe SC this can be a consequence of spin, charge, or orbital fluctuations [51]. (The nature of magnetic interactions and their interplay with orbital degrees of freedom in Fe SC is reviewed in a separate contribution to this issue [67].) However, an inquiry into the origin of this interaction is related to the question as to what triggers the nematic transition. To the best of our knowledge, this issue is not entirely settled for all the Fe-based systems, and is beyond the scope of the current review. Instead, here we adopt a more phenomenological point of view whereby, assuming the existence of such a transition, we write down a minimal effective theory that describes the transition and the critical phenomenon associated with it. It is in this low-energy effective theory sense that one should understand the above interaction term.

The last term,

$$V = V_0 \sum_{\mathbf{k},\mathbf{q},\sigma} c^{\dagger}_{\mathbf{k}+\mathbf{q},\sigma} c_{\mathbf{k},\sigma}\,, \tag{6}$$

describes scattering of electrons with isotropic point-like impurity potentials. The role of this term is to provide a finite lifetime to the electrons. In the following, the impurity term does not affect the description of the charge nematic instability. However, the inclusion of finite lifetime is crucial for a meaningful discussion of the Raman response function. In a perfect metal, where quasi-particles are infinitely long-lived, the Raman response, involving intra-band particle–hole excitations and zero momentum transfer with the photons, vanishes. This is due to the fact that the constraints from energy and momentum conservation cannot be satisfied simultaneously. Adding impurity scattering is an effective way to bypass the latter, and to take into account the intra-band contribution that is always, in practice, present.

2.2. Instability and critical fluctuations

We first discuss the effect of the impurity scattering. We assume that the impurity potential is weak enough to be treated in Born's approximation. This provides a finite lifetime to the electrons given by

$$\tau^{-1} = 2\pi n_i V_0^2 \rho_0, \tag{7}$$

where n_i is the impurity concentration, and ρ_0 is the density of states at Fermi energy.

Next, we treat the interaction in random phase approximation. The description of the charge nematic instability is facilitated by introducing the Hubbard–Stratanovich field $\phi_n(\mathbf{q})$ to decouple the interaction, which can be rewritten as

$$\mathcal{H}_I = \frac{g_0}{2} \sum_{\mathbf{q}} [\phi_n(-\mathbf{q})\phi_n(\mathbf{q}) + \phi_n(-\mathbf{q}) O_n(\mathbf{q})] \tag{8}$$

The second term above describes the interaction between electrons and the Hubbard–Stratanovich field $\phi_n(\mathbf{q})$, which is shown graphically in Fig. 2(a). With this rearrangement, the theory is formally quadratic in the fermionic variables, which can be integrated out. This leads to the action in terms of the critical variable

$$S[\phi_n] = \sum_{\mathbf{q},\mathrm{i}\nu_n} \chi_n^{-1}(\mathbf{q}, \mathrm{i}\,\nu_n)\, |\phi_n(\mathbf{q}, \mathrm{i}\nu_n)|^2\,, \tag{9}$$

where $\chi_n(\mathbf{q}, \mathrm{i}\,\nu_n)$ is the nematic susceptibility given by

$$\chi_n^{-1}(\mathbf{q}, \mathrm{i}\nu_n) = g_0\,[1 - g_0 \Pi_n(\mathbf{q}, \mathrm{i}\nu_n)]\,, \tag{10}$$

with the nematic polarization

$$\Pi_n(\mathbf{q}, \mathrm{i}\,\nu_n) = -\frac{2}{\beta} \sum_{\omega_n,\mathbf{k}} f^2_{\mathbf{k},\mathbf{q}} G_{\mathbf{k}}(\mathrm{i}\omega_n) G_{\mathbf{k}+\mathbf{q}}(\mathrm{i}\,\omega_n + \mathrm{i}\nu_n) \tag{11}$$

In the above $\beta = 1/(k_B T)$, where k_B is the Boltzmann constant, and the factor 2 is due to the summation over the spin index. The electron Green's function is given by

$$G_{\mathbf{k}}(\mathrm{i}\,\omega_n)^{-1} = \mathrm{i}\,\omega_n - \epsilon_{\mathbf{k}} + \mathrm{i}/(2\tau)\,\mathrm{sgn}(\omega_n) \tag{12}$$

Note that, since the impurity potential is isotropic, for symmetry reasons the vertex correction due to impurity scattering affects neither the $\mathbf{q} \to 0$ limit of $\chi_n(\mathbf{q}, 0)$, which controls the charge nematic transition temperature, nor the susceptibility $\chi_n(0, \mathrm{i}\,\nu_n)$, which will be relevant when we discuss the Raman response in the next section. Consequently, in the current model, the role of the impurity is restricted to providing finite lifetime to the electronic excitations.

It is convenient to divide the frequency and momentum dependencies of the nematic polarization into two parts, namely the contributions from the high-energy and the low-energy electrons, such that

$$\Pi_n(\mathbf{q}, \mathrm{i}\,\nu_n) = \Pi_n(0,0) + \Pi_n(\mathbf{q}, \mathrm{i}\,\nu_n)_{\text{high}} + \Pi_n(\mathbf{q}, \mathrm{i}\,\nu_n)_{\text{low}} \tag{13}$$

Since we do not expect any singular contribution from the high-energy electrons, the resulting frequency and momentum dependence is analytic. To lowest order, we expect

$$\Pi_n(\mathbf{q}, \mathrm{i}\,\nu_n)_{\text{high}} = c_1 (q/k_{\mathrm{F}})^2 + c_2 (\nu_n/E_{\mathrm{F}})^2 \tag{14}$$

In the above, $\Pi_n(0,0)$ and the coefficients $c_{1,2}$ depend on the details of the band structure. The charge nematic transition takes place when the Stoner criterion

$$r_0 \equiv 1 - g_0 \Pi_n(0,0) = 0 \tag{15}$$

is satisfied. In general r_0, which is related to the nematic correlation length ξ_n by $r_0 = (a/\xi_n)^2$ with a being the unit cell length, is temperature dependent and it decreases as the nematic correlation length increases upon approaching the instability with lowering temperature. In electron-doped Ba122, it is now known from elastic constant measurements (discussed in a separate contribution to this issue [55]) and also from Raman scattering measurements (described later in this review) that r_0 is linear in temperature over a wide range, i.e.

$$r_0(T) = \tilde{r}_0 (T - T_0), \tag{16}$$

where T_0 is the charge nematic transition temperature.

The low-energy contribution $\Pi_n(\mathbf{q}, \mathrm{i}\,\nu_n)_{\text{low}}$ determines the dynamical properties of the charge nematic fluctuations, and its evaluation is quite standard. The $\epsilon_{\mathbf{k}}$-integral can be performed by linearizing the electronic dispersion. This gives to leading order

$$\Pi_n(\mathbf{q}, \mathrm{i}\,\nu_n)_{\text{low}} = -\mathrm{i}\,\nu_n \rho_0 \int_0^{2\pi} \frac{\mathrm{d}\theta_{\mathbf{k}}}{2\pi} \frac{h_{\mathbf{k}}^2}{\mathrm{i} S_{\nu_n} - v_{\mathrm{F}}\, q \cos(\theta_{\mathbf{k}} - \theta_{\mathbf{q}})}$$

In the above, $S_{\nu_n} = \nu_n + \mathrm{sgn}(\nu_n)/\tau$, v_{F} is Fermi velocity, and $\theta_{\mathbf{k}}$ is the angle of $\mathbf{k}$ measured from one of the two equivalent major axes of the unit cell. The angular integral can be performed analytically if we approximate the B_{1g} form factor by $h_{\mathbf{k}} \approx -\cos(2\theta_{\mathbf{k}})$. From the angular integral, we get

$$\begin{aligned} \Pi_n(\mathbf{q}, \mathrm{i}\,\nu_n)_{\text{low}} = \frac{\mathrm{i}\,\nu_n \rho_0}{v_{\mathrm{F}} q} \Big[& \cos^2(2\theta_{\mathbf{q}}) I_{\mathrm{C}}(a_{\mathbf{q},\nu_n}) \\ & + \sin^2(2\theta_{\mathbf{q}}) I_{\mathrm{S}}(a_{\mathbf{q},\nu_n}) \Big], \end{aligned} \tag{17}$$

where $a_{\mathbf{q},\nu_n} = [\nu_n + \mathrm{sgn}(\nu_n)/\tau]/(v_{\mathrm{F}} q)$,

$$\begin{aligned} I_{\mathrm{C}}(a) &\equiv -\int_0^{2\pi} \frac{\mathrm{d}\theta}{2\pi} \frac{\cos^2 2\theta}{\mathrm{i}\,a - \cos\theta} \\ &= \mathrm{i}(1 + 2a^2) \left[\frac{(1+2a^2)}{\sqrt{1+a^2}} \mathrm{Sgn}(a) - 2a \right], \end{aligned} \tag{18}$$

and

$$\begin{aligned} I_{\mathrm{S}}(a) &\equiv -\int_0^{2\pi} \frac{\mathrm{d}\theta}{2\pi} \frac{\sin^2 2\theta}{\mathrm{i}\,a - \cos\theta} \\ &= 2\,a\,\mathrm{i} \left[1 + 2a^2 - 2\,|a| \sqrt{1+a^2} \right] \end{aligned} \tag{19}$$

Thus, the overall $\mathbf{q}$-dependence of the nematic polarization is anisotropic, which is eventually a consequence of the form factor associated with the nematic variable defined in Eq. (4) [68]. In the above, the ratio $a_{\mathbf{q},\nu_n}$ is large for temporal fluctuations and it is small for spatial fluctuations.

Quasi-static limit, $a_{\mathbf{q},\nu_n} \ll 1$: This limit is relevant for studying the thermodynamic signatures of the charge nematic instability. Using the properties

$$I_C(a \to 0) = \mathrm{i}\,\mathrm{sgn}(a) - 2\,\mathrm{i}\,a,$$

$$I_S(a \to 0) = 2\,\mathrm{i}\,a,$$

we get in this limit

$$\chi_n^{-1}(\mathbf{q}, \mathrm{i}\,\nu_n) = g_0 \left[r_0 + c_1 \frac{q^2}{k_F^2} + c_2 \frac{\nu_n^2}{E_F^2} + 2c_3 \frac{|\nu_n|}{v_F q} \cos^2 2\theta_{\mathbf{q}} - 4c_3 \frac{\nu_n^2}{(v_F q)^2} (1 + (|\nu_n|\,\tau)^{-1}) \cos 4\theta_{\mathbf{q}} \right], \tag{20}$$

with $c_3 = g_0\,\rho_0$.

Quasi-dynamical limit, $a_{\mathbf{q},\nu_n} \gg 1$: This limit is relevant for studying the signatures of the critical mode $\phi_n(\mathbf{q})$ in Raman spectroscopy [69]. This is because, in typical Raman scattering experiments, the momentum $\mathbf{q}$ given to the electrons by the visible photons is negligible compared to the Fermi momentum. Using

$$I_C(a \to \infty) = I_S(a \to \infty) = \mathrm{i}/(2a),$$

we get in this limit

$$\chi_n^{-1}(\mathbf{q}, \mathrm{i}\,\nu_n) = g_0 \left[r_0 + c_1 \frac{q^2}{k_F^2} + c_2 \frac{\nu_n^2}{E_F^2} + c_3 \frac{|\nu_n|}{|\nu_n| + 1/\tau} \right] \tag{21}$$

In this limit, the momentum anisotropy is absent from the leading order terms.

Analyticity of $\chi_n(0,0)$: From Eqs. (20) and (21) it is important to note that $\chi_n(0,0)$ obtained from the static and the dynamic limits are the same, i.e., for an infinitesimal $\eta > 0$

$$\lim_{q\to 0} \lim_{\omega \to 0} \chi_n(\mathbf{q}, \omega + \mathrm{i}\,\eta) = \lim_{\omega \to 0} \lim_{q \to 0} \chi_n(\mathbf{q}, \omega + \mathrm{i}\,\eta) = \frac{1}{g_0 r_0} \tag{22}$$

This implies that $\chi_n(\mathbf{q}, \omega + \mathrm{i}\,\eta)$ is analytic at zero momentum and frequency.

As a quick aside, the above behavior is to be contrasted with the susceptibility of a conserved quantity such as the charge susceptibility, which as we will show below is not what is measured in the Raman response. The charge susceptibility is defined by

$$\chi_c(\mathbf{q}, \mathrm{i}\,\nu_n) \equiv \int_0^\beta \langle T_\tau\, \rho_{-\mathbf{q}}(\tau) \rho_{\mathbf{q}}(0) \rangle \mathrm{e}^{\mathrm{i}\,\nu_n \tau} \tag{23}$$

where T_τ is the imaginary time ordering operator, and

$$\rho_{\mathbf{q}} \equiv \sum_{\mathbf{k},\sigma} c^\dagger_{\mathbf{k}+\mathbf{q},\sigma} c_{\mathbf{k},\sigma} \tag{24}$$

is the Fourier component of the charge-density operator. In this case, it is well known that the uniform charge susceptibility from the static limit is finite with

$$\lim_{\mathbf{q}\to 0} \chi_c(\mathbf{q}, 0) = \chi_c \neq 0, \tag{25}$$

where χ_c is the charge compressibility of the electronic system. On the other hand, the dynamical limit vanishes with

$$\chi_c(0, \omega + \mathrm{i}\,\eta) = 0 \tag{26}$$

This is a consequence of particle number conservation, i.e., $\left[\mathcal{H}, \rho_{\mathbf{q}=0}\right] = 0$, which in turn follows from the global $U(1)$ symmetry of the Hamiltonian. In other words, this symmetry enforces a non-analyticity at zero frequency and momentum, and

$$\lim_{q\to 0} \lim_{\omega \to 0} \chi_c(\mathbf{q}, \omega + \mathrm{i}\,\eta) \neq \lim_{\omega \to 0} \lim_{q \to 0} \chi_c(\mathbf{q}, \omega + \mathrm{i}\,\eta) \tag{27}$$

By contrast, the uniform nematic operator is not a conserved quantity, since $[\mathcal{H}_I, O_n(\mathbf{q} = 0)] \neq 0$, and therefore there is no physical reason to expect a similar non-analyticity in $\chi_n(\mathbf{q}, \omega + \mathrm{i}\,\eta)$ at zero frequency and momentum in *purely electronic models*, i.e., those where the coupling of the electrons to the lattice strains is ignored. As we discuss in the next section, the analyticity implied by Eq. (22) is important for interpreting the signature of the charge nematic instability in Raman response.

Note that, in order to establish the analyticity of $\chi_n(0,0)$, it is crucial to consider electrons with finite lifetime. It is easy to check that Eq. (22) does not hold for an ideal metal for which $\tau^{-1} \to 0$. However, such a non-analyticity, which is not associated with any symmetry, and whose origin can be traced to the fact that for an ideal metal the phase space for particle–hole excitations is sharply defined, is rather an artefact. In practice, the electrons have a finite lifetime, and this ensures that the phase space for particle–hole excitations is no longer sharply defined.

3. Theory: electronic Raman response near a charge nematic instability

In this section we discuss the characteristic signatures of a charge nematic instability in electronic Raman spectroscopy. We also discuss how electron–lattice coupling affects such an instability. We argue that the Raman response is "blind" to this coupling, and therefore it is an *ideal tool for studying the bare electronic nematic correlations*.

3.1. B_{1g} response, static and dynamic limits

The theory underlying the electronic Raman spectroscopy for correlated systems has been reviewed elsewhere [70,71]. Here, we simply remind few salient points associated with this experimental technique. Accordingly, we define the stress tensor by

$$T_{\alpha\beta}(\mathbf{q}) \equiv \sum_{\mathbf{k},\sigma} \frac{\partial^2 \epsilon_{\mathbf{k}}}{\partial k_\alpha \partial k_\beta} c^\dagger_{\mathbf{k}+\mathbf{q}/2,\sigma} c_{\mathbf{k}-\mathbf{q}/2,\sigma} \tag{28}$$

and the associated correlator as

$$\chi_{\alpha\beta}(\mathbf{q}, \mathrm{i}\,\Omega_n) \equiv \int_0^\beta \mathrm{d}\tau \, \langle T_\tau T^\dagger_{\alpha\beta}(\mathbf{q},\tau) T_{\alpha\beta}(\mathbf{q},0)\rangle \, \mathrm{e}^{\mathrm{i}\,\Omega_n \tau} \tag{29}$$

Following Kubo formalism, the analytic continuation of the above gives the response function

$$\begin{aligned} \chi_{\alpha\beta}(\mathbf{q},\Omega) &= \lim_{\mathrm{i}\,\Omega_n \to \Omega + \mathrm{i}\,\eta} \chi_{\alpha\beta}(\mathbf{q}, \mathrm{i}\,\Omega_n) \\ &= i \int_0^\infty \mathrm{d}t \, \mathrm{e}^{\mathrm{i}\,\Omega t} \langle \Big[T^\dagger_{\alpha\beta}(\mathbf{q},t) \ , \ T_{\alpha\beta}(\mathbf{q},0) \Big] \rangle \end{aligned} \tag{30}$$

The imaginary part of the stress tensor response function at its dynamical limit, i.e., $\chi''_{\alpha\beta}(\mathbf{q}=0,\Omega) \equiv \mathrm{Im}\,\chi_{\alpha\beta}(\mathbf{q}=0,\Omega)$, is accessible by means of Raman scattering experiment. This is because the associated scattering cross-section is proportional to the correlation function $S_{\alpha\beta}(\Omega) \equiv \langle T^\dagger_{\alpha\beta}(\Omega) T_{\alpha\beta}(\Omega)\rangle$, which in turn satisfies the fluctuation–dissipation theorem

$$S_{\alpha\beta}(\Omega) = \frac{1}{\pi} \left[1 + n_{\mathrm{B}}(\Omega)\right] \chi''_{\alpha\beta}(\mathbf{q}=0,\Omega) \tag{31}$$

where $n_{\mathrm{B}}(\Omega)$ is the Bose function.

In the Fe SC, using the notations of a unit cell with 1Fe/cell, the quantity of interest is the B_{1g} stress tensor given by

$$T_{\mathrm{B}_{1g}}(\mathbf{q}) \equiv T_{xx}(\mathbf{q}) - T_{yy}(\mathbf{q}) \tag{32}$$

Within the effective mass approximation [72], valid for non-resonant Raman scattering, we define the associated Raman vertex as

$$\gamma_{\mathrm{B}_{1g}}(\mathbf{k}) \equiv \left(\partial^2_{k_x} - \partial^2_{k_y}\right) \epsilon_{\mathbf{k}} = 2 t_1 h_{\mathbf{k}} \tag{33}$$

where the dispersion of Eq. (2) is given by $\epsilon_{\mathbf{k}} = -2t_1(\cos k_x + \cos k_y) + \cdots$, with t_1 being the nearest-neighbor hopping parameter. In principle, $\gamma_{\mathrm{B}_{1g}}(\mathbf{k})$ can include higher harmonics of the same B_{1g} symmetry, such as that coming from the third nearest-neighbor hopping, if present in $\mathcal{H}_0$. In the following, we ignore such terms since they do not affect the results qualitatively.

The computation of the B_{1g} correlator within random phase approximation (RPA) is quite straightforward. We get

$$\chi_{\mathrm{B}_{1g}}(\mathbf{q}, \mathrm{i}\,\Omega_n) = \Pi_{\gamma\gamma}(\mathbf{q}, \mathrm{i}\,\Omega_n) + g_0^2 \Pi^2_{\gamma h}(\mathbf{q}, \mathrm{i}\,\Omega_n) \chi_n(\mathbf{q}, \mathrm{i}\,\Omega_n) \tag{34}$$

where $\Pi_{\gamma\gamma}$ is defined like Π_n in Eq. (11) with the form factors $f^2_{\mathbf{k},\mathbf{q}}$ replaced by $\gamma^2_{\mathrm{B}_{1g}}(\mathbf{k})$, and $\Pi_{\gamma h}$ is defined similarly with the form factors $\gamma_{\mathrm{B}_{1g}}(\mathbf{k}) h_{\mathbf{k}}$. The graphical representation of these two terms is shown in Fig. 2(b). Note that the second term, which contains the critical contribution, is non-zero only in the Raman B_{1g} channel. In the A_{1g} and the B_{2g} channels, this term is zero by symmetry. Indeed, in experiments the signature of the charge nematic instability is observed only in the B_{1g} Raman channel. Since, $\Pi_{\gamma\gamma} = 4 t_1^2 \, \Pi_n$, and $\Pi_{\gamma h} = 2 t_1 \, \Pi_n$, we get, at low frequency and momentum

$$\chi_{\mathrm{B}_{1g}}(\mathbf{q}, \mathrm{i}\,\Omega_n) \approx 4 t_1^2 \, \chi_n(\mathbf{q}, \mathrm{i}\,\Omega_n) \tag{35}$$

The above proportionality implies that the properties of $\chi_n(\mathbf{q}, \mathrm{i}\,\Omega_n)$, discussed in Section 2, are also relevant for $\chi_{\mathrm{B}_{1g}}(\mathbf{q}, \mathrm{i}\,\Omega_n)$ (see also [73,74]). In particular, in *purely electronic models* the B_{1g} response function is analytic at zero frequency and momentum.

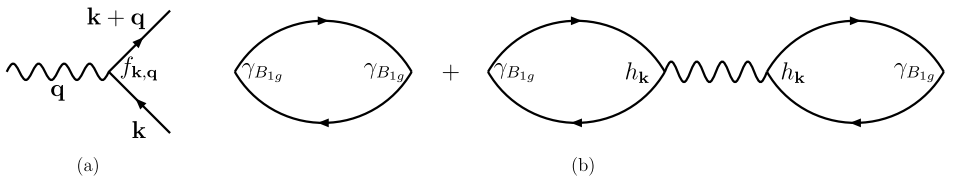

Fig. 2. (a) Interaction between electrons (solid lines) and the charge nematic boson (wavy line) ϕ_n. The interaction vertex has a non-trivial momentum dependence given by $f_{\mathbf{k},\mathbf{q}} = (h_{\mathbf{k}} + h_{\mathbf{k}+\mathbf{q}})/2$ with the B_{1g} form factor $h_{\mathbf{k}} = \cos k_x - \cos k_y$. (b) Graphs for the Raman response function. The first term is the quasi-particle contribution, which is non-critical. The second term is the contribution of the nematic boson, which has information about criticality associated with the nematic instability. This contribution is non-zero, only in the B_{1g} Raman channel.

In electronic Raman spectroscopy in the B_{1g} geometry, we measure a quantity proportional to $\chi''_{B_{1g}}(\mathbf{q}=0,\Omega) \equiv \mathrm{Im}\,\chi_{B_{1g}}(\mathbf{q}=0,\Omega)$. This quantity can be used to deduce the frequency-integrated spectral weight of the associated Raman conductivity $\chi''_{B_{1g}}(\mathbf{q}=0,\Omega)/\Omega$, which, by the Kramers–Kronig relation, gives the real part of the uniform response function. Thus,

$$\begin{aligned}\chi^{\text{dynamic}}_{B_{1g}} &\equiv \frac{2}{\pi}\int_0^\infty \frac{d\Omega}{\Omega}\chi''_{B_{1g}}(\mathbf{q}=0,\Omega)\\ &= \lim_{\Omega\to 0}\chi_{B_{1g}}(\mathbf{q}=0,\Omega)\end{aligned} \tag{36}$$

It is important to distinguish the two conceptually distinct quantities $\chi^{\text{dynamic}}_{B_{1g}}$ and

$$\chi^{\text{static}}_{B_{1g}} \equiv \lim_{\mathbf{q}\to 0}\chi_{B_{1g}}(\mathbf{q},\Omega=0) \tag{37}$$

Note that the thermodynamic instability at a charge nematic transition is associated with a divergence in the latter quantity. However, since $\chi_{B_{1g}}(\mathbf{q},\Omega)$ is analytic at zero frequency and momentum in purely electronic systems, we get

$$\chi^{\text{dynamic}}_{B_{1g}} = \chi^{\text{static}}_{B_{1g}}, \tag{38}$$

and, therefore, the divergence is "visible" from the dynamical limit. In other words, one can obtain information about the divergence of a susceptibility associated with the charge nematic instability from Raman spectroscopy.

3.2. Signature of instability: quasi-elastic peak

In the following, we study the low-frequency properties of the Raman response near the transition. Using Eqs. (21) and (35), for $\Omega \lesssim 1/\tau \ll E_F$, we get

$$\chi_{B_{1g}}(\mathbf{q}=0,\Omega) = A_0\left[r_0 + c_3\frac{\Omega}{\Omega + i/\tau}\right]^{-1} \tag{39}$$

with $A_0 = 4t_1^2/g_0$ and $c_3 = g_0\rho_0$. This implies a Raman response with

$$\chi''_{B_{1g}}(\mathbf{q}=0,\Omega) = \frac{A_0 c_3 \tau^{-1}}{(r_0+c_3)^2}\left(\frac{\Omega}{\Omega^2+\Gamma^2}\right) \tag{40}$$

where

$$\Gamma = \frac{r_0}{(r_0+c_3)\tau} \tag{41}$$

Thus, the characteristic signature of the transition in the low frequency Raman conductivity is a quasi-elastic peak with a Lorentzian lineshape that sharpens as the system approaches the transition, since the width $\Gamma \to 0$.

It is useful to note that the $\chi^{\text{dynamic}}_{B_{1g}}$ deduced from the experimental data [75] (described in Section 5) has the form

$$\chi^{\text{dynamic}}_{B_{1g}} = \frac{A_0}{r_0} + B \tag{42}$$

where B is a non-singular part that is often temperature independent. This apparent violation of the Kramers–Kronig relation is partly due to the fact that, in practice, the upper cutoff of the frequency integral of Eq. (36) is finite and is set to a value beyond which the measured Raman spectra is temperature independent. A second reason for the B-term is that part of the electronic Raman signal observed is symmetry independent and therefore unrelated to criticality.

Finally, we note that, besides $\chi^{\rm dynamic}_{\rm B_{1g}}$ and the width Γ, a third quantity that is experimentally accessible is the slope of the Raman response at zero frequency,

$$S_l \equiv \left[\partial_\Omega \chi''_{\rm B_{1g}}(\mathbf{q}=0,\Omega)\right]_{\Omega=0} = \frac{A_0\, c_3\, \tau}{r_0^2} \tag{43}$$

where the equality is the result of the random phase approximation. Using $\Gamma \approx r_0/(c_3\tau)$ close enough to the phase transition, we get a scaling relation between the three experimentally accessible quantities

$$\chi^{\rm dynamic}_{\rm B_{1g}} = \Gamma S_l \tag{44}$$

provided we ignore the non-singular B-term in Eq. (42). This provides an independent check for the validity of the random phase approximation theory.

3.3. Effects of coupling with the lattice

A crucial ingredient in the above discussion is the analyticity of the nematic susceptibility $\chi_n(\mathbf{q}, \mathrm{i}\,\Omega_n)$, and therefore that of the correlator $\chi_{\rm B_{1g}}(\mathbf{q}, \mathrm{i}\,\Omega_n)$ involving the $\rm B_{1g}$ stress tensor, at zero momentum and frequency. It is this property that allows us to conclude that the thermodynamic divergence at the charge nematic phase transition, which shows up in the susceptibility taken to its static limit, is also "visible" from the dynamic limit that is accessible via Raman spectroscopy. As we discussed earlier, in order to demonstrate the analyticity, it is important to consider electrons having a finite, frequency-independent lifetime, which, in simplest models, can be typically attributed to impurity scattering.

The above conclusion, however, holds only if we ignore the symmetry-allowed coupling of the electronic charge nematic operator $O_n(\mathbf{q})$ of Eq. (4) with the orthorhombic strain of the underlying lattice. In practice, however, such electron–lattice coupling is always present in crystalline solids. In the Fe SC, the fact that the C_4 symmetry breaking (ignoring the positions of the As and the chalcogen atoms) is invariably accompanied by orthorhombic distortion, provides phenomenological proof of the presence of such a coupling. Consequently, it is worthwhile to examine how the above statements concerning the charge nematic transition and its Raman "visibility" are modified once the coupling with the elastic strain is taken into account.

In the following, we consider a two-dimensional square lattice whose elastic free energy, to lowest order in the strains, is given by

$$F_{\rm E} = \frac{C_{11}}{2}\left(\epsilon_{xx}^2 + \epsilon_{yy}^2\right) + \frac{C_{66}}{2}\epsilon_{xy}^2 + C_{12}\epsilon_{xx}\epsilon_{yy} \tag{45}$$

Here $\epsilon_{ij} \equiv (\partial_i u_j + \partial_j u_i)/2$, with $(i, j) = (x, y)$ are the strains, the vector $\mathbf{u}$ denotes displacement from equilibrium, and C_{11} etc. denote elastic constants in Voigt notation.

In terms of the above, the orthorhombic strain is given by $\epsilon_S(\mathbf{r}) \equiv \epsilon_{xx}(\mathbf{r}) - \epsilon_{yy}(\mathbf{r})$, and the accompanying bare elastic constant is $C_{\rm S}^0 \equiv (C_{11} - C_{12})/2$. We write the symmetry-allowed coupling between the orthorhombic strain and the electronic charge nematic operator $O_n(\mathbf{q})$ as

$$\mathcal{H}_{\rm el-lattice} = \lambda_0 \sum_{\mathbf{q}} O_n(\mathbf{q})\epsilon_S(\mathbf{q}), \tag{46}$$

where $\epsilon_S(\mathbf{q})$ is the Fourier transform of $\epsilon_S(\mathbf{r})$, and λ_0 is the coupling constant having the dimension of energy.

Studying the detailed implications of the above coupling on an electronic nematic phase transition is beyond the scope of the current review, and will be presented elsewhere. Here we focus only on the following salient points that are relevant to the current discussion.

(i) One effect of the coupling is to increase the temperature of the C_4 symmetry breaking nematic/orthorhombic transition from T_0, defined in Eq. (16), to

$$T_{\rm S} = T_0 + \lambda_0^2/(C_{\rm S}^0 \tilde{r}_0\, g_0) \tag{47}$$

Below $T_{\rm S}$ the C_4 symmetry breaking is manifested both in the electronic sector, where the dispersions becomes C_2 symmetric, as well as in the lattice sector with orthorhombicity $\epsilon_{\rm S} \neq 0$. Note that the effective orthorhombic elastic constant can be expressed as (for a derivation see, e.g., Ref. [55])

$$C_{\rm S} = C_{\rm S}^0 - \lambda_0^2 \chi_n(0,0) \tag{48}$$

where $\chi_n(\mathbf{q}, \omega)$ is the bare electronic nematic susceptibility defined in Eq. (10). This implies that $C_{\rm S}$ vanishes at $T = T_{\rm S}$, and consequently the transition can be detected in experiments that measure $C_{\rm S}$ either directly by ultrasound or indirectly by bending techniques.

(ii) At $T_{\rm S}$, only the effective orthorhombic elastic constant $C_{\rm S}$ vanishes, while the remaining elastic constants stay finite. An important consequence of this is that the critical fluctuations are restricted to two high-symmetry lines $q_x = \pm q_y$ in the two-dimensional Brillouin zone [76,77]. This can be understood from the following. Writing $q_1 = (q_x + q_y)/\sqrt{2}$, it can

be shown that along the lines $q_x = q_y$ and for the polarizations $\mathbf{n}_1 = (1, -1)$ the acoustic phonon dispersion is given by $\Omega_{1,\mathbf{q}} = (C_S/\rho)^{1/2} q_1$, where ρ is the atomic mass density. Similarly, along $q_x = -q_y$ and for the polarization $\mathbf{n}_2 = (1, 1)$ the dispersion is $\Omega_{2,\mathbf{q}} = (C_S/\rho)^{1/2} q_2$, where $q_2 = (q_x - q_y)/\sqrt{2}$. It can be shown that these are the only two directions in the Brillouin zone for which the phonon velocity vanishes at T_S. This is because for all other $\mathbf{q}$ the acoustic phonons excite not just the critical strain ϵ_S, but also the non-critical ones whose elastic constants remain finite at T_S.

(iii) Finally, and most importantly for the current discussion, as a result of the electron–lattice coupling, the nematic susceptibility acquires a non-analytic correction. Denoting the dressed susceptibility as $\bar{\chi}_n$, for $\mathbf{q} = q_\alpha \hat{q}_\alpha$ (summation not implied) with $\alpha = (1, 2)$, we get that

$$\bar{\chi}_n^{-1}(q_\alpha \hat{q}_\alpha, \mathrm{i}\,\Omega_n) = \chi_n^{-1}(q_\alpha \hat{q}_\alpha, \mathrm{i}\,\Omega_n) - \frac{\lambda_0^2 q_\alpha^2}{C_S^0 q_\alpha^2 + \Omega_n^2} \tag{49}$$

Here $\hat{q}_\alpha$ are the unit vectors along the two critical directions within the Brillouin zone. The non-analyticity of the second term is a consequence of translation symmetry. Since moving all the atomic positions by a fixed displacement does not change the overall energy of the system, the electron phonon coupling, which is the numerator of the second term above, vanishes in the uniform limit $q_\alpha \to 0$. As a consequence, the effect of the acoustic phonons is entirely absent in the dynamical limit and $\bar{\chi}_n(\mathbf{q} = 0, \Omega) = \chi_n((\mathbf{q} = 0, \Omega))$.[1] In other words, the Raman response, being opaque to the acoustic phonons, measures the *bare electronic nematicity* and $\chi_{\mathrm{B_{1g}}}^{\mathrm{dynamic}} \propto (T - T_0)^{-1}$ deduced from it tends to diverge at the purely electronic temperature scale T_0 [69]. This is in contrast to the inverse of the orthorhombic elastic constant $C_S^{-1} \propto (T - T_S)^{-1}$. However, the divergence of $\chi_{\mathrm{B_{1g}}}^{\mathrm{dynamic}}$ is invariably cutoff at the actual C_4 symmetry-breaking transition T_S. Conversely, since the electronic Raman response function is unaffected by the acoustic phonons, any *signature of nematicity seen in Raman is unambiguous proof that it is electronic in origin*.

3.4. Extension to multi-orbital systems

Until now, the qualitative physics was described in terms of a single band system in order to simplify the discussion. Nevertheless, it applies equally well to multi-orbital (and multi-band) systems like Fe SC. In a multi-orbital environment, the main additional novelty is that, due to the presence of the orbital quantum number, one can construct different flavors of charge nematic order parameters. The most direct extension of the single band case described in Eq. (4) is a multi-orbital version of the d-wave Pomeranchuk instability where the orbitally resolved electron densities have all $\mathrm{B_{1g}}$ nematic form factors:

$$O_o^d \equiv \frac{1}{\sqrt{\mathcal{N}}} \sum_{m,\mathbf{k}} h_{\mathbf{k}} n_{\mathbf{k}}^m \tag{50}$$

where $n_{\mathbf{k}}$ is the electron density operator, m is the orbital index, and $h_{\mathbf{k}} = \cos k_x - \cos k_y$. While little discussed initially, this instability has recently been put forward as a candidate order parameter for the orthorhombic phase of FeSe [79–81]. A second possibility is to define a orbital dependent order parameter of the form:

$$O_o^s \equiv \frac{1}{\sqrt{\mathcal{N}}} \sum_{\mathbf{k}} g_{\mathbf{k}} (n_k^{xz} - n_k^{yz}) \tag{51}$$

involving the xz and the yz orbitals. Here $g_{\mathbf{k}}$ is a function with $\mathrm{A_{1g}}$ symmetry such as $g_{\mathbf{k}} = 1$ (equivalent to xz/yz ferro-orbital order [28–30,82]), or $g_{\mathbf{k}} = \cos k_x + \cos k_y$. Note that the actual deformations of the Fermi pockets in the nematic phase, and the axis along which a pocket will elongate/contract, can vary depending on the choice of $g_{\mathbf{k}}$. In a two-orbital model relevant for Fe SC, the deformations obtained with $g_{\mathbf{k}} = 1$ are qualitatively similar to that obtained with a non-zero d-wave Pomeranchuk order parameter O_o^d. One reason for this is that the electron pockets comprised mostly of the xz and the yz orbitals are centered around $(\pi, 0)$ and $(0, \pi)$, respectively, and the form factor $h_{\mathbf{k}}$ is approximately a constant, with opposite signs for these pockets. Consequently, the projections of these two order parameters on the electron pockets are indistinguishable. The various Fermi surface deformations associated with different choices of the nematic order parameter are illustrated in Fig. 3.

Overall, we notice that in a multi-orbital system the nematic order parameter can have non-trivial structure in the orbital space, and it can also be accompanied by momentum space structures that are different than what is possible in the single-band case described by Eq. (4). From the point of view of Raman spectroscopy, it is important to note that, irrespective of the details of their momentum and of the orbital space structures, as long as the nematic order parameter

[1] The in-plane wave-vector transferred is indeed very small in actual Raman experiments, typically $q \sim 6.10^{-3}$ nm^{-1}, making finite $\mathbf{q}$ effects unobservable in the energy range probed experimentally. The out-of-plane wave-vector transferred can be significantly larger due to the finite penetration depth of the incoming visible photons. We note however the out-of-plane component of $\mathbf{q}$ is irrelevant for the coupling with the orthorhombic strain which is purely in-plane (see Eq. (49)).

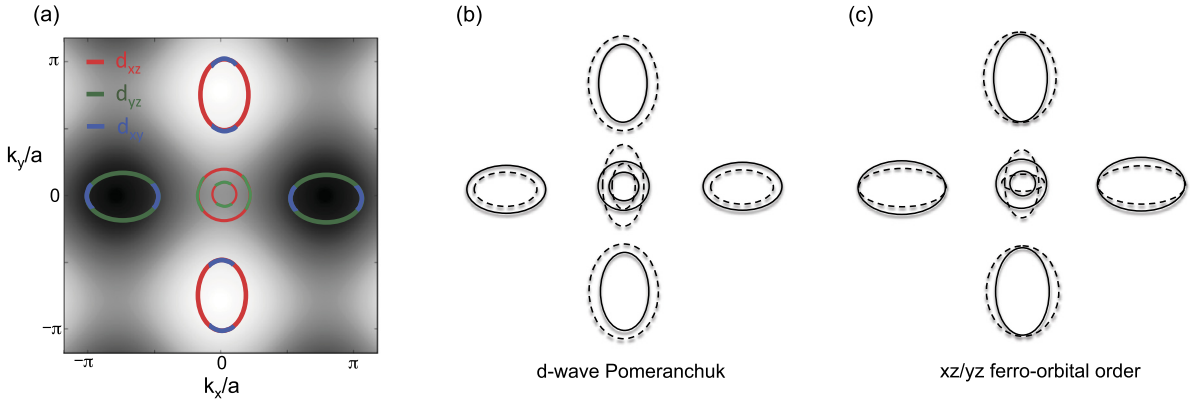

Fig. 3. (a) Typical Fermi surface of most Fe SC within a 3-orbital tight binding model (see, e.g., Daghofer et al. [78]). The orbital content of each pocket is indicated. The B_{1g} form factor $\cos k_x - \cos k_y$ is depicted in the background. (b) Fermi surface deformation associated with the d-wave Pomeranchuk order O_o^d. (c) Fermi surface deformation associated with xz/yz ferro-orbital order O_o^s with $g_k = 1$ [28,29].

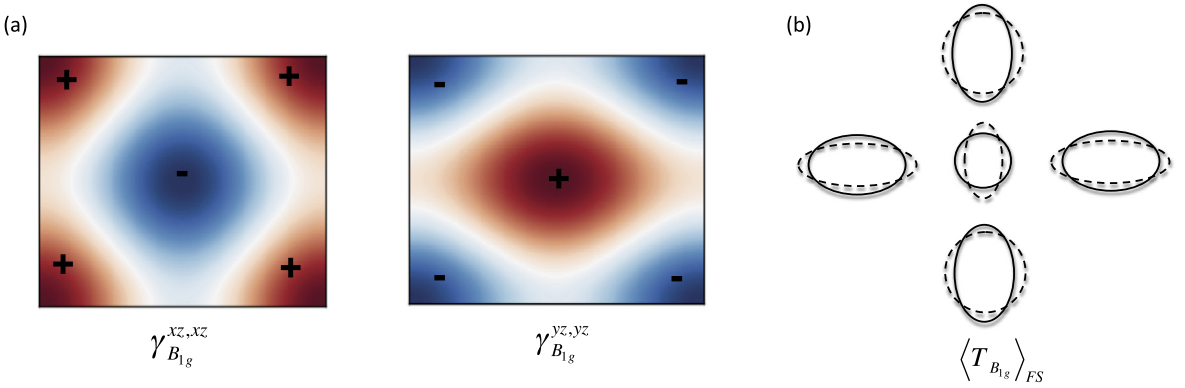

Fig. 4. (a) k-Space structure of the B_{1g} Raman vertex matrix elements in the orbital basis for the two orbital model of Raghu et al. [84] (see also [83] for a more realistic 5-band calculation of the Raman vertex). In this simplified model, the main features of the Fermi surface topology of Fe SC can be reproduced with $t_2 = -1.3\,t_1$. (b) Fermi surface deformation associated with the corresponding B_{1g} average stress tensor projected at the Fermi wave-vectors within the 2-orbital model.

transforms as a B_{1g} object, the critical fluctuations will be observable in the electronic Raman B_{1g} channel. This can be illustrated by calculating the form of the B_{1g} stress tensor or vertex for a specific tight binding model of the Fe SC. In a multi-orbital system, one can generalize Eq. (33) and write the component of the non-resonant B_{1g} Raman vertex in the effective mass approximation [83]

$$\gamma_{B_{1g}}^{mn} \equiv \left(\partial_{k_x}^2 - \partial_{k_y}^2\right) \epsilon_{\mathbf{k}}^{mn} \tag{52}$$

where ϵ_k^{mn} are the components of the tight binding dispersion in the orbital basis. In the minimal two-orbital (m, $n = d_{xz}$, d_{yz}) model of the Fe SC of Raghu et al. [84], the B_{1g} vertex is diagonal in orbital space with

$$\gamma_{B_{1g}}(\mathbf{k}) = \begin{pmatrix} 2(t_1 \cos k_x - t_2 \cos k_y) & 0 \\ 0 & 2(t_2 \cos k_x - t_1 \cos k_y) \end{pmatrix} \tag{53}$$

where t_1 and t_2 are the near-neighbor hopping parameters for σ- and π-type Fe orbital overlap, respectively. We note that next nearest-neighbor hopping integral along the diagonals of the Fe square plane do not contribute to the B_{1g} Raman vertex. The k-space structure of the two diagonal Raman vertex matrix elements and the associated Fermi surface deformation is illustrated in Fig. 4 for the tight binding parameters of Raghu et al. [84].

In this model, the B_{1g} stress tensor is

$$T_{B_{1g}}(\mathbf{q} = 0) = (t_1 + t_2) O_o^d + (t_1 - t_2) O_o^s \tag{54}$$

with $g_{\mathbf{k}} = \cos k_x + \cos k_y$. The B_{1g} stress tensor has finite overlap with both the ferro-orbital and the d-wave Pomeranchuk order parameters, and therefore criticality in either of these two channels is manifested in the Raman B_{1g} response. Conversely, based on the Raman data, it is difficult to determine whether the nematic criticality is ferro-orbital or of d-wave Pomeranchuk type.

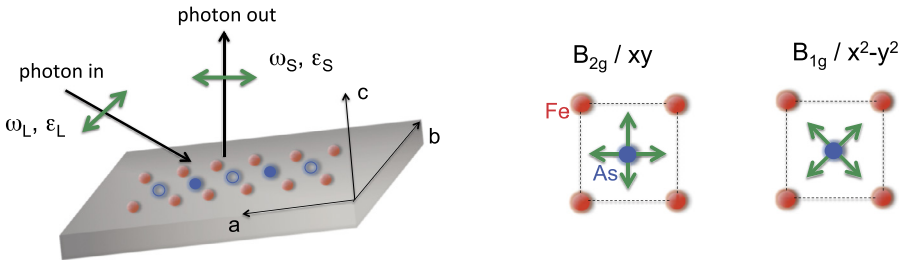

Fig. 5. Sketch of the scattering geometry in a Raman experiment. The photon polarization configuration corresponding to the B_{1g} and B_{2g} symmetries are depicted with respect to the FeAs plane. Note that the 1 Fe unit cell notation is used.

3.5. Summary of the theoretical discussion

Here we summarize the main points of the theory developed in the previous and in the current sections. In Section 2, we developed a Drude–RPA theory to describe a charge nematic or *d*-wave Pomeranchuk phase transition, starting from a phenomenological electron–electron interaction. In particular, we showed that in purely electronic models, the nematic susceptibility $\chi_n(\mathbf{q}, \Omega)$, which describes static and dynamic fluctuations of the charge nematic operator $O_n(\mathbf{q})$, is analytic at zero momentum and frequency, provided that we take into account the effect of impurity-induced elastic scattering of the electrons on their lifetimes. The latter ensures that the single particle scattering rate does not vanish at zero frequency, which is a crucial ingredient in order to establish the analyticity. We also noted that this analyticity is eventually tied to the fact that the uniform charge nematic operator $O_n(\mathbf{q} = 0)$ is not a conserved quantity. Next, in Section 3 we discussed the characteristic signatures of the charge nematic instability in the electronic Raman response. Within the Drude–RPA theory, the effect of the criticality is symmetry-selective in the sense that it is observed only in the Raman B_{1g} channel, and not in the other Raman channels. We showed that the B_{1g} Raman response $\chi''_{B_{1g}}(\Omega)$ is proportional to the imaginary part of the nematic susceptibility in its dynamical limit, i.e., to $\mathrm{Im}\,\chi_n(\mathbf{q} = 0, \Omega)$. Next, using the analyticity discussed above, as well as the Kramers–Kronig relation, we argued that the frequency-integrated Raman conductivity $\chi''_{B_{1g}}(\Omega)/\Omega$ is a measure of the nematic susceptibility at its static limit, i.e., $\lim_{\mathbf{q}\to 0} \chi_n(\mathbf{q}, \Omega = 0)$, which is the quantity whose divergence signals the second-order charge nematic transition. Furthermore, we showed that when the single particle lifetime is dominated by elastic scattering, the B_{1g} Raman conductivity has a Lorentzian lineshape, whose width narrows as a function of temperature as the system approaches the nematic instability. Finally, we pointed out that the electronic Raman response function naturally screens out the effect of the coupling of the electronic nematic variable with the orthorhombic strain of the lattice. Consequently, the Raman response is a measure of the bare electronic nematicity that is unaffected by the presence of the lattice. As such, it is an ideal tool for providing qualitative distinction between an electronically-driven nematic instability from a lattice-driven one.

4. Raman experiments

Raman scattering is a photon-in–photon-out process in which an incident photon with energy ω_L and polarization ϵ_L is inelastically scattered by the medium into a photon of energy ω_S and polarization ϵ_S (Fig. 5). For a Stokes process, $\omega_S < \omega_L$, an excitation with energy $\omega = \omega_L - \omega_S$ is created in the solid. ω is usually referred to as the Raman shift and is traditionally given in units of cm^{-1} ($8.066\ \mathrm{cm}^{-1} = 1$ meV). A typical Raman spectrum for a metal consists of sharp peaks due to Raman allowed optical phonons superimposed on a continuum of electronic origin. The Raman experiments described here were carried out using a diode-pumped solid state laser emitting at 532 nm or an Ar–Kr mixed gas laser with several lines in the visible spectral range. The inelastically scattered photons were analyzed using a triple-grating spectrometer equipped with a nitrogen-cooled CCD camera. Special care was taken in order to determine the laser induced heating. It was first estimated by comparing the power and temperature dependencies of the phonon frequencies. This estimate was then cross-checked by monitoring the onset of Rayleigh scattering by orthorhombic structural domains across the structural transition temperature as a function of laser power. For Co–Ba122 crystals, both methods yielded an estimated heating of $1\ \mathrm{K} \pm 0.2$ per mW of incident power. In order to extract the imaginary part of the Raman response function, the raw spectra were corrected for the Bose factor using Eq. (31) and for the instrumental spectral response as well.

In this review, we will mostly discuss the spectra performed in the B_{1g} symmetry because they probe the nematic degrees of freedom relevant to the Fe SC. The $x^2 - y^2$ or B_{1g} symmetry can be selected by choosing crossed incoming and outgoing photon polarizations at 45 degrees with respect to the Fe–Fe bonds. Here the notation B_{1g} refers to the one Fe unit cell whose axes are along the Fe–Fe bonds. For comparison, we will also show spectra in B_{2g} symmetry that can be selected by choosing incoming and outgoing photon polarizations along the Fe–Fe bonds. Switching between both symmetries was usually performed by rotating the crystal by 45 degrees while keeping both the polarizer and the analyzer fixed. Note that in terms of the full lattice unit cell (or 2 Fe unit cell), which has its axes at 45 degrees to the Fe–Fe bonds and is sometimes used in the literature, the B_{1g} (B_{2g}) symmetry discussed here corresponds to the B_{2g} (B_{1g}) symmetry.

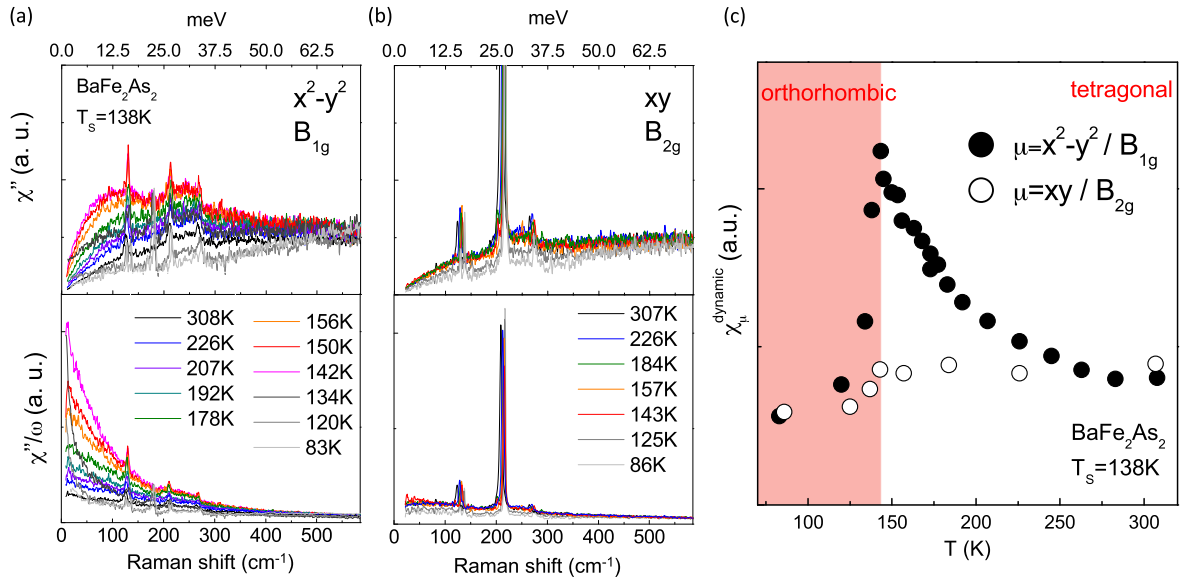

Fig. 6. Raman responses χ'' and Raman conductivity χ''/ω in the B_{1g} (a) and B_{2g} (b) symmetry of $BaFe_2As_2$. The sharp lines superimposed on the electronic continuum are due to Raman active optical phonon excitations. (c) Temperature dependence of the extracted static nematic susceptibilities in the two symmetry channels using the Kramers–Kronig relation (see text).

5. Experiments: charge nematic susceptibility of electron-doped 122 systems

5.1. Electron-doped $Ba(Fe_{1-x}Co_xAs)_2$

We first discuss Raman data in the normal state of electron-doped $Ba(Fe_{1-x}Co_xAs)_2$ (Co–Ba122) and the evolution of the extracted static nematic susceptibility as a function of temperature and Co doping [75]. Being one of the most studied Fe SC system, the salient features of the phase diagram as a function of Co doping are well-known [85]. There is a quasi-simultaneous magneto-structural transition in the parent compound ($T_S \sim T_N$) [86,87], which splits under Co doping with $T_S > T_N$ [11,12,88–91]. The superconducting dome starts at $x \sim 0.02$ and extends up to at least $x = 0.15$. All the Co contents x mentioned in this review were determined using wavelength-dispersing X-ray spectroscopy (WDS).

The low-energy ($\omega < 600$ cm^{-1} or 75 meV) Raman responses of the parent compound $BaFe_2As_2$ in the B_{1g} and B_{2g} symmetries are shown as a function of temperature in Fig. 6(a) and (b). In the tetragonal phase, the B_{1g} response shows a strong enhancement upon cooling towards $T_S = 138$ K, before collapsing in the orthorhombic/spin density wave (SDW) state. By contrast, the B_{2g} response is essentially independent of temperature in the tetragonal phase and only shows a mild suppression below T_S. The observed symmetry dependence is in agreement with the presence of dynamical nematic fluctuations having $x^2 - y^2$ symmetry, as discussed above. This interpretation is confirmed by the Co doping dependence of the spectra, which shows a systematic enhancement of the B_{1g} response towards T_S and the disappearance of any temperature dependence in the strongly electron overdoped composition, far away from the orthorhombic instability ($x = 0.20$, see Fig. 7).

From the behavior of the Raman response at finite energy, one can define the associated nematic susceptibility $\chi_\mu^{\text{dynamic}}$, where μ is the symmetry channel, using Kramers–Kronig relation (see Eq. (36)). As emphasized above, the susceptibility is in this case obtained in the dynamical limit. The physical quantity governing the nematic susceptibility in this limit, the Raman conductivity χ''/ω, is shown as a function of symmetry for Ba122 in Fig. 6. It is also shown as a function of electron Co doping in Fig. 7. While the Raman conductivity is flat in B_{2g} symmetry, in B_{1g} symmetry it is dominated by a peak centered at zero energy over a wide range of Co doping in the tetragonal phase. For $x \leq 0.045$, the peak amplitude grows upon approaching T_S and collapses quickly below. It is interesting to note that the enhancement of the peak amplitude is also seen down to the superconducting phase, $T \sim T_c$, for $x = 0.065$ and also, albeit more moderately, for $x = 0.10$. At these two compositions, no T_S is observed, and the system remains tetragonal and paramagnetic down to $T = 0$ K [88,92,93]. Data in the SC state will be discussed in Section 7.

The Raman conductivity being independent of temperature for $\omega > 600$ cm^{-1} in the tetragonal phase, the quantity $\chi_\mu^{\text{dynamic}}$ can be extracted in both symmetries by first extrapolating the data from the lowest energy measured (9 cm^{-1} $\sim$ 1 meV) down to 0 cm^{-1}, and then integrating up to 600 cm^{-1}. The symmetry dependence of this quantity is shown in Fig. 6(c) for the parent compound Ba122. While the values of $\chi_\mu^{\text{dynamic}}$ are very similar at high temperature in B_{1g} and B_{2g} symmetries, the enhancement of the susceptibility upon cooling is only seen in B_{1g} symmetry, clearly indicating an instability towards a charge nematic order with B_{1g} or $x^2 - y^2$ symmetry.

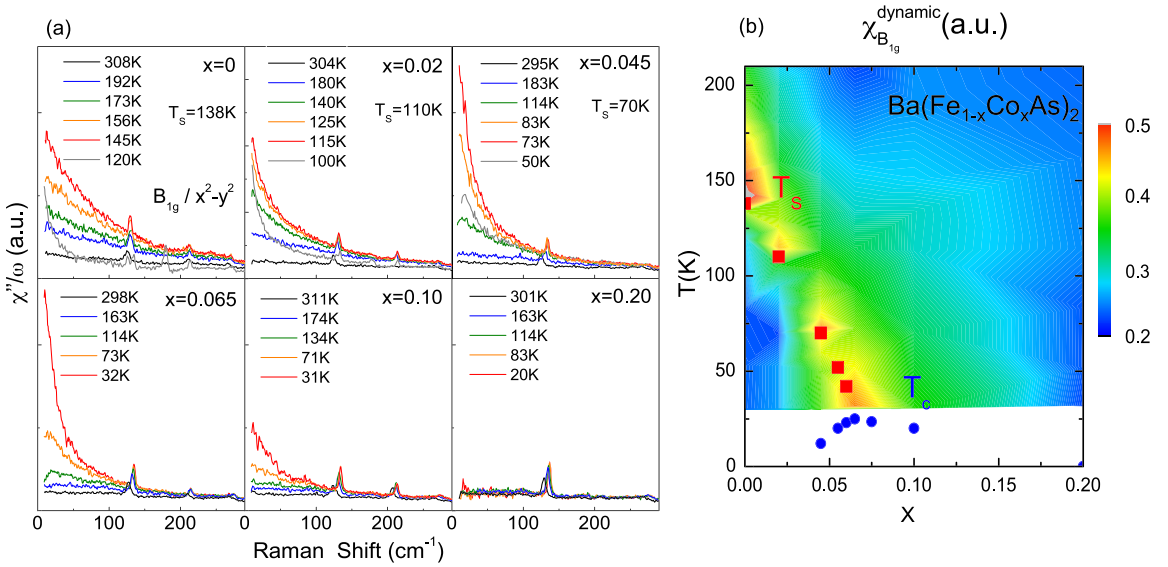

Fig. 7. (a) Temperature dependence of the Raman conductivity χ''/ω in the B_{1g} symmetry of $Ba(Fe_{1-x}Co_xAs)_2$ (Co–Ba122) for different Co doping concentrations x. (b) Color plot of the nematic susceptibility $\chi^{\text{dynamic}}_{B_{1g}}$ as a function of temperature and Co doping.

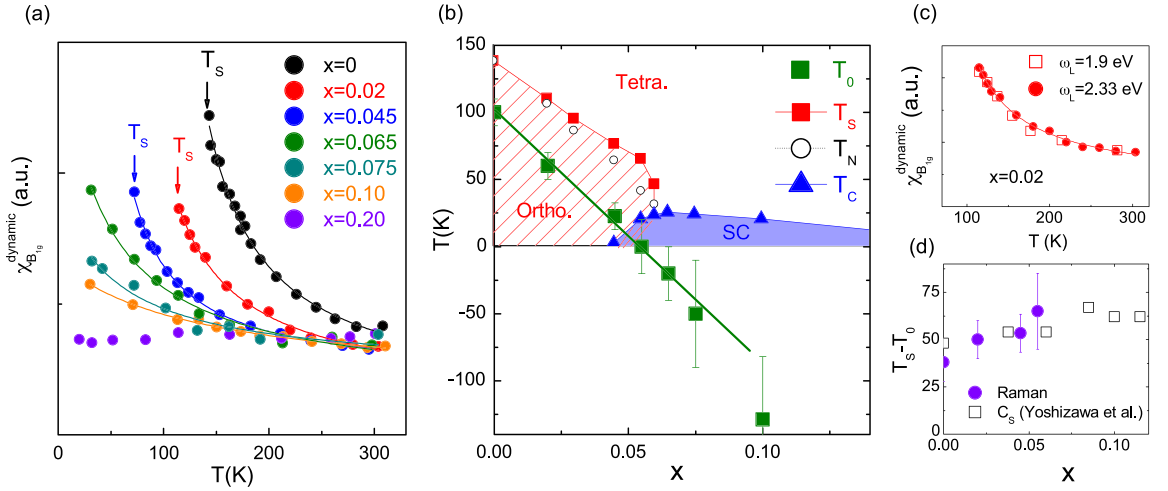

Fig. 8. (a) Curie–Weiss fits of the nematic susceptibility in the tetragonal phase of Co–Ba122. Structural transition temperatures T_S are marked by arrows for $x \leq 0.045$. (b) Phase diagram showing the Co doping dependence of the bare electronic nematic Curie–Weiss temperature T_0 (green squares). (c) Temperature dependence of the nematic susceptibility deduced from measurements at two different incident photon energies for $x = 0.02$ ($T_S = 110$ K). (d) Co doping dependence of the difference between the measured structural transition temperature T_s and T_0. The open squares correspond to the same quantity extracted from a Curie–Weiss analysis of the shear modulus C_s by Yoshizawa et al. [53].

The Co doping and temperature dependencies of $\chi^{\text{dynamic}}_{B_{1g}}$ are summarized in the color plot shown in Fig. 7(b). The plot shows the clear correlation between the maximum of $\chi^{\text{dynamic}}_{B_{1g}}$ and T_s. It also highlights the persistence of significant nematic fluctuations over a wide range of Co doping covering most of the superconducting dome.

As shown in Fig. 8(a) for each Co composition, the nematic susceptibility can be well fitted using a Curie–Weiss law (see Eq. (16) in Section 2.2 and Eq. (42) in Section 3.2):

$$\chi^{\text{dynamic}}_{B_{1g}} = B + \frac{C}{T - T_0} \tag{55}$$

where $C = \frac{A_0}{r_0}$ is a temperature-independent constant.

Here B is a constant that describes the temperature- and symmetry-independent part of the susceptibility, i.e. the non-critical part of the Raman response, and T_0 is the Curie–Weiss temperature corresponding to the lattice-free electronic

nematic transition temperature as defined in Section 2.2. The extracted values of T_0 follow qualitatively the doping dependence of T_S and extrapolate to zero slightly below optimal doping, at the critical doping $x = x_c \sim 0.055$ (Fig. 8(b)). As displayed in Fig. 8(c) for $x = 0.02$, the temperature dependence of the nematic susceptibility does not depend appreciably on the incident photon energy ω_L used for the Raman experiment. The insensitivity to ω_L suggests that the resonant terms in the Raman vertex, if present, do not alter appreciably the temperature behavior of the B_{1g} response above T_S, justifying the use of the effective mass approximation as done in Eq. (33) of Section 3.1 and in Eq. (52) of Section 3.4.

It is important to note that the T_0 values are systematically at least 40 K below the actual thermodynamic structural transition temperature T_S. This difference is a natural consequence of the absence of contribution of the lattice to the extracted susceptibility, as discussed in Section 3.3. T_0 represents the bare nematic transition temperature of the purely electronic system, while in the presence of the lattice, the actual transition temperature T_S is moved to higher temperature due to the finite coupling λ_0 between the electronic and lattice sub-systems (see Eq. (47)). In that case the observed divergence of the nematic susceptibility is therefore cut-off by the structural transition that occurs at $T_S > T_0$. The difference between the two temperatures is a measure of the charge–lattice coupling energy $\lambda_0^2/(c_S^0 \tilde{r}_0 g_0)$. This quantity, which is accessible both from Raman and from elastic constant measurements, is shown as a function of Co doping in Fig. 8(d).

5.2. Comparison with elastoresistivity and elastic measurements

The observed Curie–Weiss-like enhancement of the charge nematic susceptibility is qualitatively consistent with both elastoresistivity and elastic modulus measurements performed on Co–Ba122 [52–54,62]. The presence of orbital fluctuations above T_S was also inferred from point-contact spectroscopy measurements in the same system [94]. In the case of elastoresistivity measurements, the purely electronic nematic susceptibility could be obtained by strain-dependent measurements of the resistivity anisotropy in the tetragonal phase [62]. The extracted divergence was taken as evidence of an electronic-driven structural transition. Since the nematic susceptibility extracted from Raman measurements is free from lattice effects, they also confirm the present of diverging electronic nematic degrees of freedom in the tetragonal phase of undoped and electron-doped Ba122. We note, however, that the Curie–Weiss temperatures extracted from transport measurements are significantly higher than the ones obtained from Raman measurements on samples with similar Co doping. The discrepancy could be due to different couplings with electronic nematic degrees of freedom. Indeed, while Raman scattering couples with charge nematic degrees of freedom, the nematic component of the elastoresistivity tensor is a more complex quantity. On the one hand, it could be a measure of Drude-weight anisotropy arising from the sensitivity of the electronic structure to generate anisotropy in the presence of external strain [95]. On the other hand, elastoresistivity is also sensitive to anisotropy in transport lifetimes of the carriers that can arise from scattering with the spin fluctuations or the impurities [37,38,64,96–99]. Deviations from the Curie–Weiss behavior have also been recently reported in several Fe SC near optimal doping by elastoresistivity measurements [100]. They have been interpreted as due to random field disorder, which is a relevant perturbation near a quantum critical nematic transition.

Elastic modulus measurements (discussed in a separate contribution in this issue [55]) can also be fitted with a Curie–Weiss-like temperature dependencies. While Young's modulus measurements by the three-point bending technique are now available for different Fe SC systems and doping values [54,101], direct measurements of the shear modulus C_S from ultrasound velocity measurements are only available for Co–Ba122 [23,52,53]. In both types of measurements, a Curie–Weiss like softening is observed in Co–Ba122. The extracted Curie–Weiss temperatures are very close to T_S, which is consistent with a second-order structural phase transition. We note that recent neutron scattering measurements in parent 122 compounds also observe a clear softening of the associated transverse acoustic phonon at low wavevectors [102]. Assuming a simple Landau-type approach of the coupling between shear modulus and electronic nematic degrees of freedom identical to the one presented in Section 3.3, the bare electronic nematic transition temperature could also be extracted from these elastic measurements using the relation $C_S = C_S^0(\frac{T - T_S^{CW}}{T - T_0})$, where $T_S^{CW} \sim T_S$ and T_0 is the purely electronic nematic transition temperature. The T_0 values obtained from shear modulus measurements in Co–Ba122 agree remarkably well with the ones extracted from Raman measurements [53,75].[2] For both Raman and shear modulus measurements, $T_S - T_0$ increases mildly with Co doping (see Fig. 8(d)), indicating a possible increase in the electron–lattice coupling energy scale $\frac{\lambda_0}{C_S^0 \tilde{r}_0 g_0}$ (see Eq. (47)) upon electron doping. We will come back in Section 6.3 for a more quantitative comparison between elastic and Raman measurements.

5.3. Impact of disorder: $Sr(Fe_{1-x}Co_xAs)_2$

As already stated above, mechanisms of anisotropic scattering are a possible source of the transport anisotropies [96–99], associated with lifetime effects, which have been reported in both the orthorhombic and the tetragonal phases under applied strains or stress. Indeed transport measurements performed on annealed crystals appear to show a much reduced anisotropy in the orthorhombic phase, hinting at a key role of scattering mechanisms in the observed nematicity [38]. STM

[2] We note that the T_0 extracted from Young's modulus measurements are somewhat higher for Co–Ba122 [54]. This might be due to the contribution of other non-critical components of the elastic tensor to the Young's modulus.

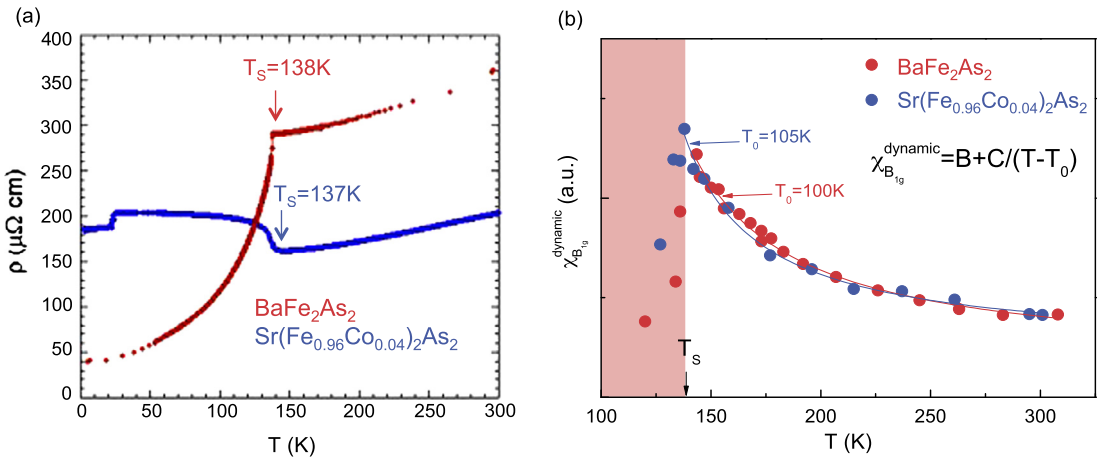

Fig. 9. (a) Temperature dependence of the resistivity of Ba122 (red, RRR∼ 9) and Co–Sr122 ($x = 0.04$, blue, RRR∼1). Unpublished data courtesy of F. Rullier-Albenque. (b) Corresponding nematic susceptibilities extracted from Raman measurement in the B_{1g} symmetry [109]. The lines are Curie–Weiss fits of the data points.

measurements have further shown the nucleation of nematic nano-domains around defect sites in the orthorhombic phase, and even possibly in the tetragonal phase [103,104]. These anisotropic impurity states were postulated to be responsible for the observed transport anisotropies because they are expected to act as strongly anisotropic scatterers [98,105,106]. Recent NMR measurements also suggest the presence of short-range but static nematic order above T_S. This short-range order could be due to pinning by impurities or to the presence of micro-strains [107], and could possibly explain the onset of anisotropy observed at $T > T_S$ in magnetic torque measurements [108].

The above measurements have raised the question of the intrinsic nature of nematicity in Fe SC. A direct comparison between the Raman measurements in Ba122 ($T_S = 138$ K) and Co–Sr122 ($x = 0.04$, $T_S = 137$ K) allows a direct assessment of the possible role of disorder in the emergence of nematic fluctuations above T_S [109]. Indeed, despite having essentially identical T_S values, the resistivity measurements shown in Fig. 9(a) indicate a much higher residual resistivity ratio (RRR) in Co–Sr122, likely caused by the insertion of Co into the FeAs plane. Despite an order of magnitude difference in RRR, the extracted nematic susceptibilities show extremely similar temperature dependencies in both systems (see Fig. 9(b)). In particular, the extracted Curie–Weiss temperatures T_0 agree within ±5 K, clearly demonstrating a relative insensibility of the nematic fluctuations and their associated diverging susceptibility to disorder. The Raman measurements are consistent with recent elasto-resistivity measurements that show that while the magnitude of the observed transport anisotropies might be disorder dependent, the diverging behavior of the extracted susceptibility in the tetragonal state is not [64]. This conclusion is supported by a recent strain-dependent optical conductivity study that suggests that the strain-induced transport anisotropy observed above T_S is not due to an anisotropic scattering rate, but rather to an anisotropic Drude weight [110]. It is likely that disorder helps revealing an underlying intrinsic nematicity in transport and local probe measurements. The magnitude of the observed anisotropies is thus not necessarily the right quantity to assess the intrinsic nematicity of a given Fe SC system.

6. Dynamical aspects of the charge nematic response

6.1. Quasi-elastic peak

We now go beyond the static properties of the nematic susceptibility discussed in the previous section, and analyze the frequency dependence of the nematic fluctuation spectrum revealed by the Raman measurements in B_{1g} symmetry. The temperature and symmetry dependencies of the Raman response in Ba122 (Fig. 6) suggest the presence of two contributions. The first one, broad in energy and weakly temperature dependent, is seen in both symmetries and dominates the Raman responses at high temperature. It can be assigned to intra and/or interband quasiparticles excitations that do not become critical upon cooling. This contribution shows only a weak suppression in the orthorhombic phase, which is linked with the simultaneous opening of the SDW gap. The second contribution, only present in B_{1g} symmetry, is strongly temperature dependent and is responsible for the strong enhancement of the static nematic susceptibility as discussed above. This contribution, obtained by subtracting the first contribution, is shown as a function of Co doping in Fig. 10(a). The observed dynamical nematic fluctuations are quasi-elastic in nature and can be well reproduced by a damped Lorentzian lineshape of width Γ and amplitude A, in agreement with the form obtained in the theory part of this review (Eq. (40)):

$$\chi''_{\mathrm{QEP}} = A\frac{\omega\Gamma}{\omega^2 + \Gamma^2} \tag{56}$$

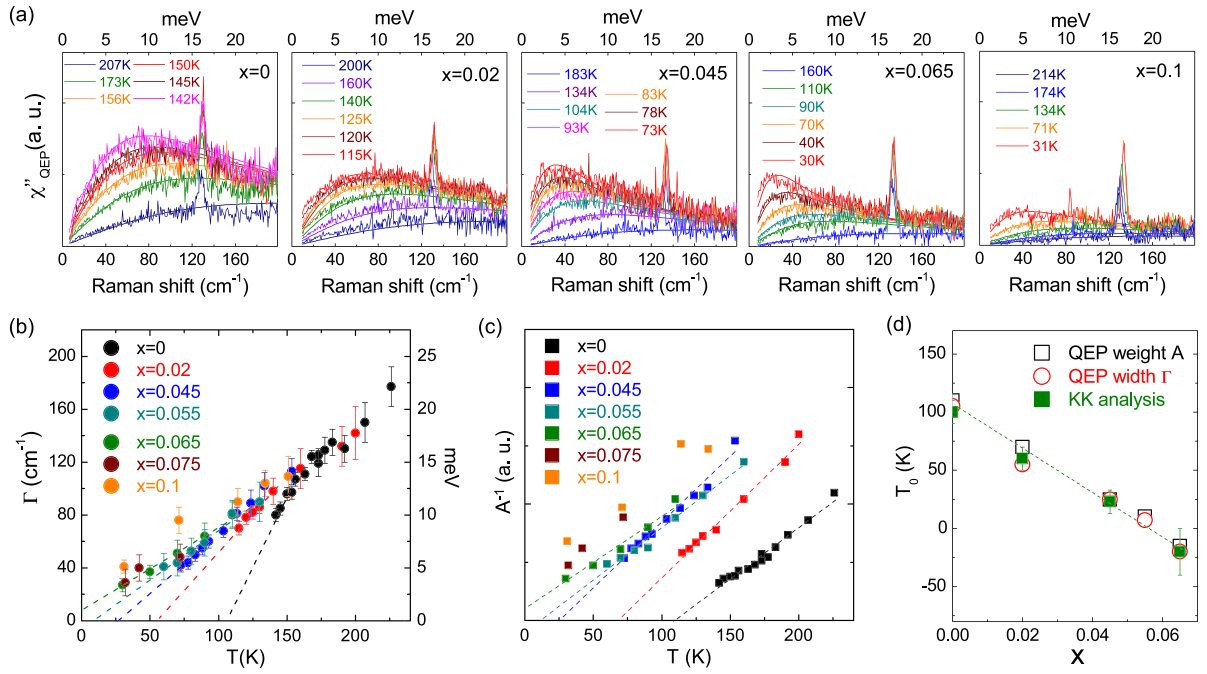

Fig. 10. (a) Evolution of the quasi-elastic peak contribution (QEP) in the B_{1g} symmetry as a function of temperature and Co doping. The contribution was extracted by subtracting the raw B_{1g} response by the one in B_{2g} symmetry for each doping. Fits using a damped Lorentzian are shown for each spectra. (b) Temperature evolution of width Γ of the quasi-elastic peak. (c) Temperature dependence of the inverse of the area A^{-1} of the QEP. (d) Co doping evolution of the mean-field nematic transition T_0 extracted by three different methods.

The temperature dependence of the width of the quasi-elastic peak (QEP) Γ is shown in Fig. 10(b). We find that Γ softens considerably upon approaching T_S for $x \leq 0.045$. This is because Γ is approximately the single particle lifetime renormalized by $(a/\xi_n)^2$, where a is the unit cell length and ξ_n is the nematic correlation length, and the latter starts to increase as the system approaches the nematic instability with lowering temperature. Assuming a Curie–Weiss T dependence of the nematic susceptibility, and sufficiently close to T_0, the temperature dependence of Γ is expected to vanish linearly with a zero intercept at T_0, the bare electronic nematic transition temperature (see Eq. (41) in Section 3.2):

$$\Gamma = \frac{r_0}{(r_0 + c_3)\tau} \propto (T - T_0) \tag{57}$$

For all Co compositions, Γ is found to decrease linearly between T_S and up to at least 40 K above T_S. As in the case of the static susceptibility, the softening of Γ is not complete because of lattice effects that move the transition temperature to a higher temperature T_S.

The above analysis also allows us to extract the temperature dependence of the QEP area A, which is directly proportional to the diverging part of the nematic susceptibility i.e. without the background non-singular contribution B in Eq. (55).

$$\chi_{B_{1g}}^{\text{dynamic,QEP}} = \frac{2}{\pi} \int_0^\infty \frac{d\omega}{\omega} \chi''_{QEP}(\omega) = A \tag{58}$$

As shown in Fig. 10(c), the temperature dependence of A^{-1} is fairly linear, as expected for a Curie–Weiss behavior, with $A^{-1} \sim (T - T_0)$. The extrapolation of the measured temperature dependencies of Γ and A^{-1} in the tetragonal phase down to zero temperature provide a measure of the scale T_0, which is in good agreement with the values obtained from the Curie–Weiss fits of the static susceptibility described in the previous section (see Fig. 10(d)).

6.2. Adequacy of RPA theory of the nematic transition

Both the frequency and the temperature dependencies of the nematic susceptibility are in broad agreement with the expectations from the simple RPA description of a charge nematic transition outlined in the theory section of this review. The fact that the diverging nematic susceptibility is interrupted by the structural transition is a direct consequence of the lack of coupling with the lattice of a nematic susceptibility extracted from Raman in the dynamic limit. Both the Curie–Weiss behavior of the susceptibility and the linear decrease with T of the effective one-particle scattering rate Γ are also in agreement with a simple mean-field description of a charge nematic instability described in Section 3.2. The RPA

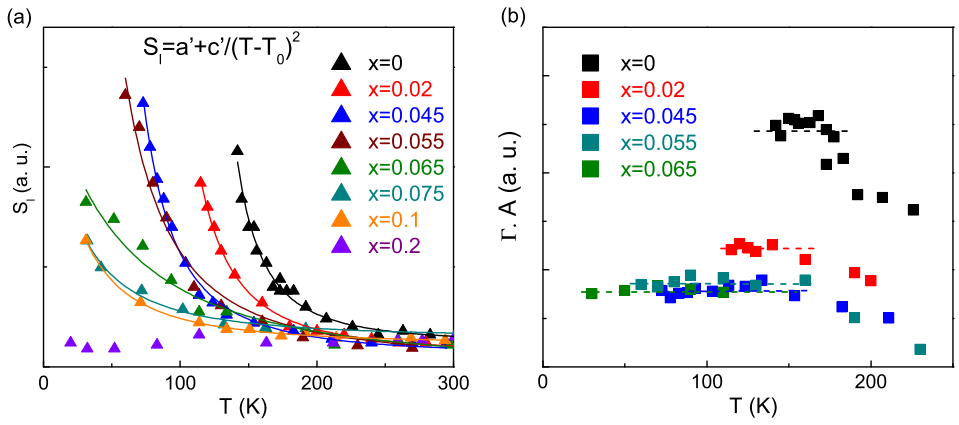

Fig. 11. (a) Temperature dependence of the slope of the Raman response at low energy S_l. The solid lines are fits using $S_l = a' + \frac{c'}{(T-T_0)^2}$. (b) Temperature dependence of the product $\Gamma \dot{A}$, where Γ is the effective one-particle scattering rate and A the diverging part of the nematic susceptibility (see text).

type picture can be further tested by looking at the low-energy slope of the B_{1g} Raman response, S_l, which is predicted to vary as $(T - T_0)^{-2}$ (see Eq. (43)). As illustrated in Fig. 11(b), the quantity S_l follows nicely the expected behavior for all Co doping values, even when forcing T_0 to the value previously obtained from the Curie–Weiss fits of the susceptibility.

A further test of the RPA picture can be made by looking at the temperature dependence of the product ΓA. Identifying Eq. (40) with Eq. (56), this product should become almost temperature independent upon approaching T_0: $\Gamma A \sim \frac{A_0}{\tau} \sim \frac{1}{g_0 \tau}$. This is indeed what is found over a wide range of Co composition as shown in Fig. 11(b). The decrease in $\frac{1}{g_0\tau}$ from $x = 0$ to $x = 0.045$ can come from different sources. It could be linked to the decrease of the bare quasiparticle scattering rate $\frac{1}{\tau}$, as suggested by transport measurements in Co–Ba122 [12,88], but it could also be due to an increase in the coupling constant g_0 upon Co-doping. Overall there is, thus, a remarkable consistency between the behavior of the nematic B_{1g} Raman response in Co–Ba122 and the theoretical expectations from a simple RPA theory of the nematic transition.

6.3. A consistent picture with shear modulus measurements

The Raman measurements indicate the presence of genuine electronic nematic fluctuations in the tetragonal phase of Co–Ba122. These fluctuations are expected to soften the lattice and trigger the structural transition [23,76]. The availability of both Raman and shear modulus data in Co–Ba122 allows us to draw a more quantitative picture linking electronic and lattice degrees of freedom. Indeed, by symmetry the charge nematic order parameter O_n probed by Raman and the orthorhombic lattice distortion ϵ_O are linearly coupled (Eq. (46)). Remembering that Raman probes the bare charge nematic susceptibility, and using Eqs. (35) and (48), we have a simple relationship between $\chi_{B_{1g}}^{\text{dynamic}}$ and C_S:

$$C_S = C_S^0 - \frac{\lambda_0^2}{4t_1^2} \chi_{B_{1g}}^{\text{dynamic}} \tag{59}$$

where λ_0 is the charge lattice coupling constant introduced in Section 3.3 and t_1 is the nearest-neighbor hopping parameter introduced after Eq. (33). Assuming a weakly temperature-dependent C_S^0, the renormalized shear modulus can become soft via the linear coupling with the charge nematic susceptibility $\chi_{B_{1g}}^{\text{dynamic}}$, causing a second-order structural phase transition at T_S defined as $C_S(T = T_S) = 0$ (see Fig. 12(a)). Fig. 12(b) shows a comparison between the shear modulus data of Yoshizawa et al. [53] and the theoretical shear modulus expected from the Raman data using equation (59), with $\lambda_0^2/(4t_1^2)$ as the only free parameter. The quantitative agreement between shear modulus data and the theoretical expectation for both undoped and Co-doped Ba122 demonstrates that the charge nematic fluctuations observed by Raman scattering can fully account for the structural softening observed in Co–Ba122. It also provides a further evidence that the structural distortion observed in Fe SC is electronic driven. We stress that such quantitative agreement cannot be reached if we assume that Raman scattering couples with the fully dressed nematic susceptibility, i.e. including lattice effects. *The realization that Raman probes the bare nematic susceptibility is therefore crucial in reaching a consistent picture.*

One question left open in our discussion until now is the role of spin degrees of freedom in the nematicity observed in Fe SC. Anisotropic spin fluctuations associated with the stripe AF instability at or below T_S of many Fe SC have been invoked early on as a main driver for nematicity [20,21]. Naively one might conclude from the consistency between shear modulus and Raman measurements that only charge/orbital degrees of freedom as probed by Raman scattering are relevant in driving the structural transition. This would however be incorrect, since it is very plausible that the diverging charge nematic susceptibility is itself enhanced or even driven by spin-nematic fluctuations via spin-charge coupling [32,111–116].

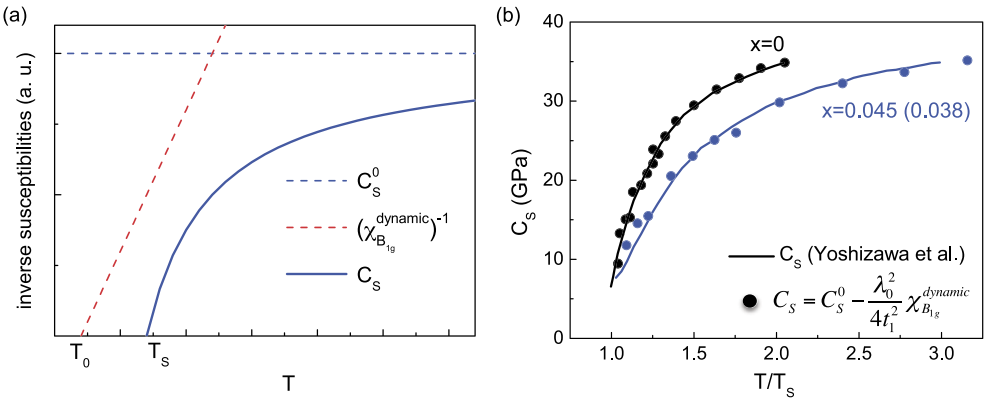

Fig. 12. (a) Mean-field model of the linear coupling between the inverse lattice (or shear modulus) and electronic nematic susceptibilities. The bare shear modulus C_S^0, initially independent of temperature, is softened by the linear coupling with a diverging nematic electronic susceptibility $\chi_{B_{1g}}^{dynamic}$ causing a phase transition at $T_S > T_0$. (b) Comparison between the experimental temperature dependence of the shear modulus C_S [53] for Co–Ba122 ($x = 0$ and $x = 0.038$) and the theoretical temperature dependence using the charge nematic susceptibility deduced from Raman measurements ($x = 0$ and $x = 0.045$, see text for details). To account for the slight mismatch in the structural transition temperatures T_S of the crystal used in the two experiments, the temperature axis was set in units of T_S.

In fact it has been argued that a similar consistency as in Fig. 11(c) can be reached by comparing NMR measurements of spin fluctuations at $Q_{SDW} = (0, \pi)/(\pi, 0)$ and shear modulus data [117]. Disentangling between the electronic degrees of freedom behind nematicity thus remains a formidable task in 122 systems [51]. Other systems like FeSe with no magnetic transition [16,18,81,101,118–120], or hole-doped Ba122 with a still mysterious C_4 magnetic phase [121–124] may prove fruitful playgrounds to answer this question. It is also possible that, like the structure of the SC gap, the respective weights of various electronic degrees of freedom behind nematicity are not universal and depend on the Fe SC systems considered.

6.4. Digression: Raman fingerprints of nematicity in cuprates

The presence of nematic correlations as possible precursor of uni-axial modulated charge/spin ordered states is also intensively discussed in the context of cuprates [125–131]. It is therefore interesting to discuss here earlier Raman data on $La_{1-x}Sr_xCuO_4$ (La-214) and $YBa_2Cu_3O_{6+\delta}$ (Y-123), which are somewhat reminiscent of the results discussed here, albeit with some key differences [65,73,132–134]. In underdoped La-214, a Raman QEP was observed to grow upon cooling over a relatively broad doping range [65]. The symmetry of the QEP was found to switch from B_{2g} to B_{1g} channels at the critical doping value $p = 0.05$, indicating a 45-degree rotation of the nematic fluctuations: along the Cu–O bond at moderate doping and at 45 degrees of the Cu–O at low doping. This is in agreement with neutron scattering studies where stripe-like spin modulations were also found to rotate upon increasing doping [135]. In La-214 there appears thus to be an intimate link between nematic ($q = 0$) fluctuations observed by Raman and finite q stripe-like charge/spin fluctuations [132,136]. This phenomenology is similar to the spin-nematic scenario for the structural transition in Fe SC discussed above. In contrast with underdoped Co–Ba122, however, the growth of the QEP in La-214 and its softening saturate at low temperature and therefore no true static long-range order sets in [65]. Besides, the growth of the QEP in La-214 is accompanied by the opening of a pseudogap at intermediate energies upon lowering temperature whose relationship with nematicity is still unclear.

In other cuprates like Y-123, $Bi_2Sr_2CaCu_2O_{8+\delta}$ and $HgBa_2CuO_{4+\delta}$ evidence for nematic fluctuations in the Raman spectra are more elusive as no clear QEP is observed for moderately underdoped systems in any symmetry [133,137,138]. Notably in moderately underdoped Y-123 where CDW fluctuations are clearly observed in X-ray measurements and where transport anisotropies have been reported, no QEP is observed in the nematic B_{1g} and B_{2g} symmetries [133,137]. It has been recently suggested that the opening of the pseudogap may suppress the nematic QEP in B_{1g} symmetry in moderately underdoped cuprates [134]. We also note that in Y-123, the question of whether the incipient order is nematic or bi-axial is still controversial [139–147]. By contrast, a clear QEP emerges in B_{2g} symmetry for strongly underdoped composition ($p < 0.05$) [133]. In this regime, however, neutron scattering data indicate the presence of uniaxial magnetic correlations along the Cu–O bond rather the Cu–O diagonal, as suggested by the B_{2g} symmetry of the Raman QEP [148]. Here again, the connection between Raman results and other probes appears problematic. The role of nematicity in cuprates and its link to the pseudogap is therefore largely unsettled, as many competing and fluctuating spin- and/or charge-ordered phases are in close proximity.

7. Nematicity and superconductivity

As of date, the study of nematicity in Fe SC has concentrated mostly on the role of the various electronic nematic degrees of freedom in driving the structural transition in the normal metallic state. Relatively less attention has been given to study the nature of these fluctuations, if at all they exist, in the superconducting phase. In the following, we show that, in a

fully-gapped superconductor, soft nematic fluctuations lead to a new collective mode whose signature is a finite frequency resonance peak in the electronic Raman response. This behavior is qualitatively different from the quasi-elastic peak that develops when the nematic transition is approached in the normal state.

A second motivation to study nematic fluctuations in the superconducting phase comes from the possibility that such fluctuations might affect the pairing mechanism and the superconducting transition. Theoretically, it has been argued that nematic fluctuations can play a role in the interplay between s and d-wave pairing states, which are likely nearly degenerate in several Fe SC systems [149–156]. Concerning the effect on pairing, recent theoretical works [157,158] suggest that nematic fluctuations enhance superconductivity irrespective of the gap symmetry, at least for weak-coupling superconductors. Therefore, it is possible that nematic fluctuations provide a complementary contribution to the pairing interaction on top of the $(\pi, 0)$ magnetic fluctuations that promote $s^{\pm}$ pairing symmetry.

On the experimental side, both X-ray measurements of the orthorhombicity and elastic modulus measurements from ultrasound velocity indicate competition between nematic and superconducting order parameters, which is in broad agreement with the expectations from simple Ginzburg–Landau-type theoretical arguments [23,52,159,160]. However, these studies did not address the question of whether the nematic/orthorhombic transition stays of the second order (or weakly of the first order) in the superconducting phase [161], and, if so, how the properties of the accompanying nematic fluctuations differ from those in the normal phase. In fact, experimental evidence of the existence of nematic fluctuations in the superconducting phase was lacking until recently. Consequently, it is notable that a recent study has identified resonance peaks in the electronic Raman response of Co-doped Ba122 and Na111 as evidence of the existence of nematic fluctuations in the superconducting phase [162].

With the above motivations, in this section we briefly discuss the theory of nematic fluctuations in a SC phase, and we compare it with the experimental findings from Raman response measurements in the SC state of electron-doped FeAs. We finish by comparing the properties of the nematic resonance mode with those of other collective modes that have been postulated to exist in the context of superconductivity in the Fe SC.

7.1. Theory: nematic resonance near a nematic quantum critical point

In the superconducting phase, the nematic fluctuations can be modeled by the same RPA approach as the one used to describe the QEP in the normal state data. As in the normal state, we assume that the nematicity is driven by an electronic interaction of the form given by Eq. (3), with the interaction constant g_0 replaced by g, its value in the superconducting phase. Within RPA, the interacting nematic susceptibility probed in B_{1g} symmetry in the superconducting state can be expressed in term of the bare superconducting response and g. It is given by (see Eqs. (10) and (34)):

$$\chi_{B_{1g}}(\omega) = \frac{\Pi_{B_{1g}}(\omega)}{1 - g\,\Pi_{B_{1g}}(\omega)} \tag{60}$$

Mathematically, it is clear that, since in the superconducting phase the Bogoliubov excitations are gapped, the structure of $\Pi_{B_{1g}}$ is quite different from that of a normal metal. For a fully gapped clean superconductor, there are no fermionic excitations below 2Δ. Consequently, the imaginary part of the bare nematic response $\Pi''_{B_{1g}}$ is zero below 2Δ, and it is dominated by a pair-breaking peak at 2Δ. It is simple to check that, by Kramers–Kronig relation, this implies that the real part $\Pi'_{B_{1g}}$ diverges logarithmically upon approaching 2Δ from below. Therefore, for a positive nematic coupling g, the RPA response develops a resonance *below* 2Δ at an energy Ω_r defined as

$$1 - g\,\Pi'_{B_{1g}}(\Omega_r) = 0 \tag{61}$$

This condition will always be met for a fully gapped superconductor in the C_4-symmetric phase near the nematic instability. Thus, the presence of a nematic resonance in the Raman spectra is a generic property of the superconducting excitation spectrum near a nematic quantum critical point. Physically, the opening of the gap shifts spectral weight from low frequencies $\omega \sim \Gamma$ in the normal phase, where Γ is the renormalized single-particle scattering rate defined in Eq. (41), to higher frequencies $\omega \sim \Delta$ in the superconducting phase. This shift of spectral weight transforms the quasi-elastic peak of the normal state into a resonance peak in the superconducting state. Close to the nematic quantum critical point, the spectral weight of this nematic resonance quickly overwhelms that of the pair-breaking peak and grows as the critical point is approached as a function of a tuning parameter such as doping [162]. The presence of a full gap is however crucial for the existence of the resonance, as nodes will effectively wash out the divergence of the real part of the bare susceptibility Π. For more details, we invite the reader to consult Ref. [162].

7.2. Experiments: fingerprints of a nematic resonance in superconducting $Ba(Fe_{1-x}Co_x)_2As_2$

Raman scattering data provide a direct insight into this problem by following the evolution of the quasi-elastic peak upon crossing T_c. Of particular interest are sample compositions that show significant nematic fluctuations down to T_c while staying in the tetragonal phase. This is illustrated for optimally doped Co–Ba122 ($x = 0.065$) in Fig. 13(a). At this composition, the low-energy B_{1g} QEP observed in the normal state (see Fig. 10) is strongly renormalized below T_c with a suppression at low energy and the emergence of a well-defined peak at finite energy in the SC state.

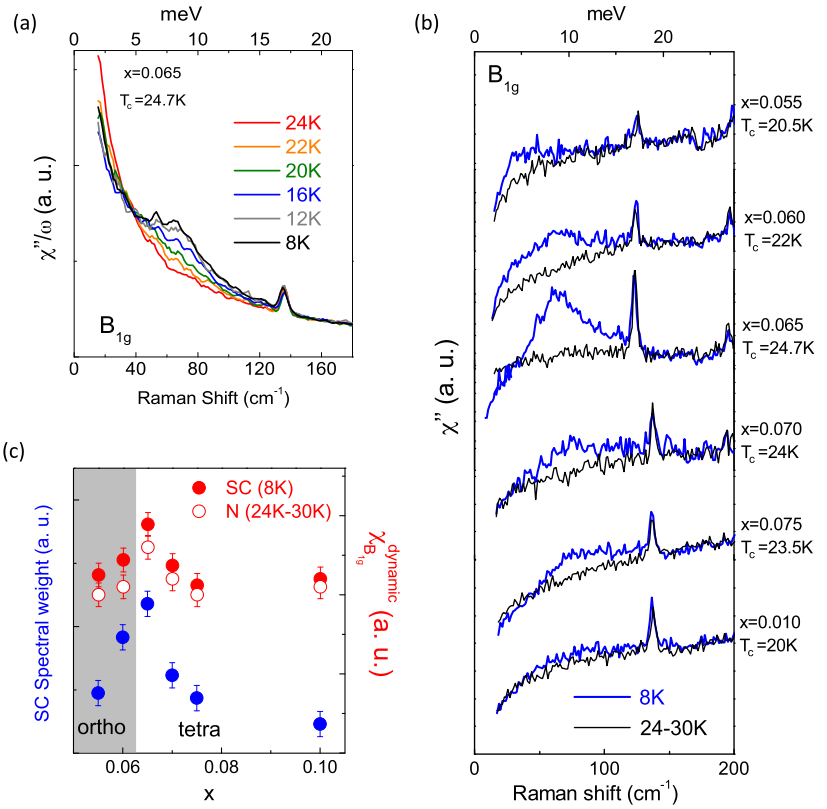

Fig. 13. (a) Evolution the B_{1g} Raman conductivity χ''/ω across T_c for Co–Ba122 ($x = 0.065$) [163]. (b) Co doping evolution of the SC B_{1g} Raman response (in blue). The responses just above T_c are shown in black. (c) Evolution of the integrated SC spectral weight of the Raman response χ'' (in blue) [163] as a function of Co doping. The corresponding nematic susceptibilities $\chi^{\text{dynamic}}_{B_{1g}}$ both at (N) and well below T_c (SC) are also shown in red.

The SC peak is only observed in B_{1g} symmetry. It was initially interpreted as a Cooper pair-breaking peak associated with the creation of pairs of Bogoliubov quasiparticles in a BCS state [163–167]. Its energy is indeed close to twice the energy gap 2Δ detected by ARPES experiments at the electron pockets in similarly doped crystals [168,169]. Its Co doping dependence however displays a striking departure from simple BCS-like expectations (see Fig. 13(b)). Coming from the tetragonal overdoped side ($x = 0.1$, $T_c = 20$ K), the SC peak spectral weight is strongly enhanced upon approaching the boundary between the tetragonal and orthorhombic phases that is located between $x = 0.065$ and $x = 0.06$ in Co–Ba122. In the nematic/SDW phase, the peak spectral weight decreases and a much weaker peak emerges at a smaller energy [163].

The strong enhancement observed on the tetragonal side ($x > 0.06$) of the phase diagram is at odds with the small changes in T_c when going from $x = 0.1$ ($T_c = 20$ K) to $x = 0.065$ ($T_c = 24.7$ K). It is also inconsistent with the fact that the peak energy actually softens towards $x = 0.065$ [163].[3] On the other hand, the doping dependence of the peak spectral weight tracks the behavior of the nematic response above T_c: it is stronger for the Co compositions when the nematic susceptibility is the strongest at $T = T_c$, i.e. close to the nematic instability (see Fig. 13(c)). This observation indicates that, as expected from the simple RPA picture discussed above, the same interaction responsible for the enhancement of the nematic susceptibility is also enhancing the SC peak spectral weight, producing a nematic resonance close to the nematic critical point. We note that a similar enhancement of a B_{1g} SC peak spectral weight has also been recently observed in electron-doped Co–Na111 upon approaching the nematic instability, indicating that the effect is possibly generic to electron-doped FeAs systems [170]. This implies that the observed peak in the superconducting B_{1g} channel is due to the nematic resonance rather than simply to non-interacting pair-breaking physics.

While the nematic resonance is essentially a delta function for a clean system, finite lifetime effects due to, e.g., disorder are expected to broaden it. The broadening can be especially significant if the resonance is not fully detached from the 2Δ pair-breaking peak. It is interesting to note the peak observed in the experiments on Co–Ba122 are significantly broader than in Co–Na111: at least 5 meV (full width at half maximum) for the former, while it can be as sharp as 1 meV for the latter [163,164,170]. This indicates that a fully detached and well-defined resonance is only present in Co–Na111, while the nematic resonance manifests itself only as a enhanced pair-breaking peak in Co–Ba122. This may reflect a stronger coupling

[3] In the BCS framework the spectral weight of the Raman pair-breaking peak should scale as Δ.

g in the case of Co–Na111, but could also be due to a larger disorder due to the higher Co concentration of optimally doped Co–Ba122.

In principle the spectral weight of the resonance is expected to diverge and its energy to go to zero at the nematic quantum critical point $x = x_c$. This corresponds to the situation where the nematic coupling reaches the critical value g_c such that the Stoner criterion is satisfied, $r_0 = 0$ (see Eq. (15)). However, because the nematic Raman response does not couple with the lattice, this does not happen: the actual thermodynamic QCP occurs before the bare nematic critical point x_c: $x_{QCP} > x_c$ or $g_{QCP} < g_c$. In Co–Ba122, x_c can be estimated by extrapolating the doping dependence of T_0: $x_c \sim 0.055$ [75,162]. x_{QCP}, on the other hand, lies at a slightly higher doping: between $x = 0.06$ and $x = 0.065$ (see Fig. 8(b)). Therefore, just like the divergence of the nematic susceptibility in the normal state is preempted by the structural transition that occurs at a higher temperature $T_S > T_0$, the complete softening of the resonance energy is also preempted by the nematic order that intervenes at a higher doping. This also explains the relatively mild softening of the mode energy seen in the experiments in Co–Ba122.

7.3. Relationship with other superconducting collective modes

The nematic resonance observed in the Raman spectrum of electron-doped Fe SC bears a strong analogy with neutron resonance observed in several families of unconventional SC. In both cases, they are due to residual electronic interactions in the particle–hole channel, which, within RPA type pictures, trigger a well-defined excitonic-like pole in the charge and spin SC responses, respectively. The nature of the residual interactions differs: magnetic and centered at finite q_{AF} for the neutron resonance, while they are centered at zero wavevector for the nematic resonance. Both resonances are connected to soft excitations associated with nearby quantum critical points: antiferromagnetic in one case and nematic in the other one. It so happens that both critical points seem to exist in Fe SC, and therefore both neutron and nematic resonances are present in their SC state. There is another key difference between both resonances: while neutron resonance requires a sign-changing gap, nematic resonance only requires the presence of a full gap. Because the presence of nodes is suspected in several Fe SC systems, it is likely that the nematic resonance will not be observed in several systems. The presence or not of a nematic resonance near the nematic instability is thus a powerful test for the presence of nodes for several systems, including, e.g., P-doped Ba122.

Finally, we should note that other collective modes have been predicted to occur in the SC state of Fe SC [171–175]. Among them, the Bardasis Schrieffer (BS) mode [172,173,176,177], an in-gap electron bound state in a sub-leading pairing channel, is the most relevant for our discussion because of the near-degeneracy of s and d-wave paring states in many Fe SC [4,150–155]. Fingerprints of its presence have been reported in the Raman spectra of optimally hole doped K–Ba122, where several sharp modes are detected below T_c [178,179]. In principle, both the nematic resonance and the BS mode can be simultaneously present in the SC Raman spectrum and may even couple [180,181]. However it is likely that their respective visibility will be strongly system dependent. While anisotropic gaps will suppress both collective modes efficiently, their presence is also linked to different criteria: the nematic resonance relies on the proximity of a nematic quantum critical point while the BS mode will occur when s and d-wave pairing states are nearly degenerate [173,182]. In this respect, we note that, from the point of view of nematicity, shear modulus and Raman scattering data show much weaker nematic fluctuations near optimally hole doped K–Ba122 where a region of C_4 magnetic phase has also been observed [54,183]. We therefore suspect that, by contrast to the electron-doped side, nematic resonance may not be present in hole-doped 122 systems, at least near optimal doping. This illustrates the remarkable richness of Fe SC where the nature of the SC ground state and its collective excitation spectrum can vary strongly from one system to the other.

8. Conclusions

The purpose of this review was two-fold. First, we have provided a general theoretical framework within which one can understand electronic Raman scattering measurements near a nematic instability. Since Raman scattering measurement in the appropriate symmetry couples directly with the nematic order parameter involving the charge degrees of freedom, we have argued that it is one of the few direct probes of nematic fluctuations in a metallic system. However, contrary to thermodynamic probes like elastic constant measurements, the electronic Raman response probes the frequency-momentum dependent nematic susceptibility in its dynamical limit. An important consequence of this is that it is essentially blind to the lattice strains and the acoustic phonons. This, in turn, implies that Raman response is an unique probe of pure electronic nematic correlations. Experimental data on electron-doped 122, and more recently 111, Fe SC systems are consistent with this theoretical picture, and therefore provide unambiguous evidence of an enhanced nematic susceptibility of electronic origin. The comparison with shear modulus data confirm the absence of coupling between the electronic Raman response and the lattice strains. It also shows that the nematic fluctuations observed in the charge sector by Raman scattering can account for the observed lattice softening in electron-doped 122, providing further evidence that the structural phase transition is electronic driven.

However, despite the encouraging consistency between different probes of nematicity in the tetragonal phase, there remain several unsolved questions. The first one is related to the issue whether the electronic nematicity is driven by spin, orbital or charge degrees of freedom. In this respect, FeSe is an interesting system because of the absence of magnetic ordering. While preliminary Raman measurements indicate the presence of charge nematic fluctuations above T_S in FeSe

[120,184], the nature of the magnetic fluctuations in this system remains to be clarified [101,185,186]. The second question is how generic are nematic fluctuations in Fe SC and whether or not they play a role in the SC pairing mechanism. Recent transport measurements advocate for the presence of underlying nematic quantum critical point near optimal doping for several systems and doping values. This will have to be confirmed by other probes and we believe electronic Raman scattering is ideally suited to answer this question. Indeed we have shown that the presence of a nematic resonance in the SC Raman response is a natural consequence of the proximity to a nematic quantum critical point, providing a smoking-gun experiment for its existence.

From a more general perspective, the discovery of nematicity in Fe SC, first revealed via transport measurements, has stimulated intense efforts to design and understand experiments capable of probing nematic degrees of freedom. These efforts can now be capitalized to search for other systems where nematic degrees of freedom have been either predicted or indirectly observed. We have already mentioned cuprates and bi-layer ruthenates in the introduction, we can also add less correlated systems like bi-layer graphene [187–189] and even bismuth [190,191]. The presence of nematic correlations can also be used to tune electronic orders via uniaxial stress or strain, just like magnetic field is routinely used to tune magnetic orders. Strain control of electronic phases has already been demonstrated in semiconductor-based heterostructures like AlAs [192,193]. In more correlated materials, strain effects have been demonstrated recently in Sr_2RuO_4, where a strong T_c enhancement under uniaxial strain was observed [194]. Up to now, the microscopic origin of these kind of effects remain relatively poorly studied however. It is therefore likely that nematicity will remain a subject of intense research in the coming years.

Acknowledgements

For the experimental results presented in this review we are indebted to the works of three PhD students, namely L. Chauvière, Y.-X. Yang, and P. Massat. We acknowledge D. Colson and A. Forget whose high-quality single crystals have been instrumental to this work, and we acknowledge F. Rullier-Albenque for sharing with us transport data. We also acknowledge R.M. Fernandes and J. Schmalian for very fruitful collaborations. Y.G. would like to thank his close collaborators within the Raman group at “Université Paris-Diderot” for their constant feedback and various technical help, namely M.-A. Méasson, M. Cazayous, and A. Sacuto. We are also grateful to E. Bascones, L. Benfatto, G. Blumberg, A. Böhmer, V. Brouet, A. Cano, R. Hackl, P. Hirschfeld, K. Ishida, M.H. Julien, H. Kontani, D. Maslov, P. Toulemonde, and B. Valenzuela for many helpful conversations. Part of this work was funded by Agence Nationale de la Recherche through ANR Grant PNICTIDES and by a SESAME Grant from “Région Île-de-France”.

References

[1] Yoichi Kamihara, Takumi Watanabe, Masahiro Hirano, Hideo Hosono, J. Am. Chem. Soc. 130 (2008) 3296.
[2] David Johnston, Adv. Phys. 59 (2010) 803.
[3] A.V. Chubukov, P.J. Hirschfeld, Phys. Today 68 (2015) 46.
[4] Kazuhiko Kuroki, Seiichiro Onari, Ryotaro Arita, Hidetomo Usui, Yukio Tanaka, Hiroshi Kontani, Hideo Aoki, Phys. Rev. Lett. 101 (2008) 087004.
[5] I.I. Mazin, D.J. Singh, M.D. Johannes, M.H. Du, Phys. Rev. Lett. 101 (2008) 057003.
[6] P.J. Hirschfeld, M.M. Korshunov, I.I. Mazin, Rep. Prog. Phys. 74 (2011) 124508.
[7] J.P. Reid, M.A. Tanatar, A. Juneau-Fecteau, R.T. Gordon, S. Rene de Cotret, N. Doiron-Leyraud, T. Saito, H. Fukuzawa, Y. Kohori, K. Kihou, C.H. Lee, H. Iyo, H. Eisaki, R. Prozorov, L. Taillefer, Phys. Rev. Lett. 109 (2012) 087001.
[8] J.-H. Chu, J.G. Analytis, K. De Greve, P.L. McMahon, Z. Islam, Y. Yamamoto, I.R. Fisher, Science 329 (2010) 824.
[9] J. Prost, P.G. de Gennes, The Physics of Liquid Crystals, Oxford Science Publication, 1974.
[10] E. Fradkin, S.A. Kivelson, M.J. Lawler, J.P. Eisenstein, A.P. Mackenzie, Annu. Rev. Condens. Matter Phys. 1 (2010) 153.
[11] N. Ni, M.E. Tillman, J.-Q. Yan, A. Kracher, S.T. Hannahs, S.L. Bud'ko, P.C. Canfield, Phys. Rev. B 78 (2008) 214515.
[12] J.-H. Chu, J. Analytis, C. Kucharczyk, I.R. Fisher, Phys. Rev. B 79 (2009) 014506.
[13] H. Luetkens, H.H. Klauss, M. Kraken, F.J. Litterst, T. Dellmann, R. Klingeler, C. Hess, R. Khasanov, A. Amato, C. Baines, M. Kosmala, O.J. Schumann, M. Braden, J. Hamann-Borrero, N. Leps, A. Kondrat, G. Behr, J. Werner, B. Büchner, Nat. Mater. 8 (2009) 305.
[14] D.R. Parker, M.J.P. Smith, T. Lancaster, A.J. Steele, I. Franke, P.J. Baker, F.L. Pratt, M.J. Pitcher, S.J. Blundell, S.J. Clarke, Phys. Rev. Lett. 104 (2010) 0571007.
[15] S. Margadonna, Y. Takabayashi, M.T. McDonald, K. Kasperkiewicz, Y. Mizuguchi, Y. Takano, A.N. Fitch, E. Suard, K. Prassides, Chem. Commun. 43 (2008) 5607.
[16] T.M. McQueen, A.J. Williams, P.W. Stephens, J. Tao, Y. Zhu, V. Ksenofontov, F. Casper, C. Felser, R.J. Cava, Phys. Rev. Lett. 103 (2009) 057002.
[17] Fong-Chi Hsu, Jiu-Yong Luo, Kuo-Wei Yeh, Ta-Kun Chen, Tzu-Wen Huang, Phillip M. Wu, Yong-Chi Lee, Yi-Lin Huang, Yan-Yi Chu, Der-Chung Yan, Maw-Kuen Wu, Proc. Natl. Acad. Sci. USA 105 (2008) 14262.
[18] T. Imai, K. Ahilan, F.L. Ning, T.M. McQueen, R.J. Cava, Phys. Rev. Lett. 102 (2009) 177005.
[19] P. Chandra, P. Coleman, A.I. Larkin, Phys. Rev. Lett. 64 (1990) 88.
[20] C. Fang, H. Yao, W.F. Tsai, J.P. Hu, S.A. Kivelson, Phys. Rev. B 77 (2008) 224509.
[21] C. Xu, M. Muller, S. Sachdev, Phys. Rev. B 78 (2008) 020501.
[22] Y. Qi, C. Xu, Phys. Rev. B 80 (2009) 094402.
[23] R.M. Fernandes, L. VanBebber, S. Bhattacharya, P. Chandra, V. Keppens, D. Mandrus, M. McGuire, B. Sales, A. Sefat, J. Schmalian, Phys. Rev. Lett. 105 (2010) 157003.
[24] I. Paul, Phys. Rev. Lett. 107 (2011) 047004.
[25] A. Cano, Phys. Rev. B 84 (Jul 2011) 012504.
[26] R.M. Fernandes, A.V. Chubukov, J. Knolle, I. Eremin, J. Schmalian, Phys. Rev. B 85 (2012) 024534.
[27] L. Fanfarillo, A. Cortijo, B. Valenzuela, Phys. Rev. B 91 (2015) 214515.
[28] Frank Krüger, Sanjeev Kumar, Jan Zaanen, Jeroen van den Brink, Phys. Rev. B 79 (2009) 054504.
[29] Chi-Cheng Lee, Wei-Guo Yin, Wei Ku, Phys. Rev. Lett. 103 (2009) 267001.

[30] C.-C. Chen, J. Maciejko, A. Sorini, B. Moritz, R. Singh, T. Devereaux, Phys. Rev. B 82 (2010) 100504.
[31] Weicheng Lv, Frank Krüger, Philip Phillips, Phys. Rev. B 82 (2010) 045125.
[32] S. Onari, H. Kontani, Phys. Rev. Lett. 109 (2012) 137001.
[33] H. Zhai, F. Wang, D.-H. Lee, Phys. Rev. B 90 (2009) 064517.
[34] J. Kang, Z. Tesanovic, Phys. Rev. B 83 (2011) 020505.
[35] M.A. Tanatar, E.C. Blomberg, A. Kreyssig, M.G. Kim, N. Ni, A. Thaler, S.L. Bud'ko, P.C. Canfield, A.I. Goldman, I.I. Mazin, R. Prozorov, Phys. Rev. B 81 (2010) 184508.
[36] J.J. Ying, X.F. Wang, T. Wu, Z.J. Xinag, R.H. Liu, Y.J. Yan, A.F. Wang, M. Zhang, G.J. Ye, P. Cheng, J.P. Hu, X.H. Chen, Phys. Rev. Lett. 107 (2011) 067001.
[37] E.C. Blomberg, M.A. Tanatar, R.M. Fernandes, I.I. Mazin, B. Shen, H.H. Wen, M.D. Johannes, J. Schmalian, R. Prosorov, Nat. Commun. 4 (2013) 1914.
[38] S. Ishida, M. Nakajima, T. Liang, K. Kihou, C.H. Lee, A. Iyo, H. Eisaki, T. Kakeshita, Y. Tomioka, T. Ito, S. Uchida, Phys. Rev. Lett. 110 (2013) 207001.
[39] S. Jiang, H.S. Jeevan, J.K. Dong, P. Gegenwart, Phys. Rev. Lett. 110 (2013) 067001.
[40] A. Dusza, A. Lucarelli, F. Pfuner, J.-H. Chu, I.R. Fisher, L. Degiorgi, Europhys. Lett. 93 (2011) 37002.
[41] M. Nakajima, T. Liang, S. Ishida, Y. Tomioka, K. Kihou, C.H. Lee, A. Iyo, H. Eisaki, T. Kakeshita, T. Ito, S. Uchida, Proc. Natl. Acad. Sci. USA 108 (2011) 12238.
[42] M. Nakajima, S. Ishida, Y. Tomioka, K. Kihou, C.H. Lee, A. Iyo, A. Ito, T. Kakeshita, H. Eisaki, S. Uchida, Phys. Rev. Lett. 109 (2012) 217003.
[43] C. Mirri, A. Dusza, S. Bastelberger, J.-H. Chu, H.H. Kuo, I.R. Fisher, L. Degiorgi, Phys. Rev. B 89 (2014) 060501.
[44] C. Mirri, A. Dusza, S. Bastelberger, J.-H. Chu, H.H. Kuo, I.R. Fisher, L. Degiorgi, Phys. Rev. B 90 (2014) 155125.
[45] Ming Yi, Donghui Lu, Jiun-Haw Chu, James G. Analytis, Adam P. Sorini, Alexander F. Kemper, Brian Moritz, Sung-Kwan Mo, Rob G. Moore, Makoto Hashimoto, Wei-Sheng Lee, Zahid Hussain, Thomas P. Devereaux, Ian R. Fisher, Zhi-Xun Shen, Proc. Natl. Acad. Sci. USA 108 (2011) 6878.
[46] Y. Kim, H. Oh, C. Kim, D. Song, W. Jung, B. Kim, H.J. Choi, C. Kim, B. Lee, H. Khim, S. ans Kim, K. Kim, J.B. Hong, Y.S. Kwon, Phys. Rev. B 83 (2011) 064509.
[47] L.W. Harriger, H.Q. Luo, M.S. Liu, C. Frost, J.P. Hu, M.R. Norman, P. Dai, Phys. Rev. B 84 (2011) 054544.
[48] X. Lu, J.T. Park, R. Zhang, H. Luo, A.H. Nevidomskyy, Q. Si, P. Dai, Science 345 (2014) 657.
[49] X. Lu, T. Keller, W. Zhang, Y. Song, J.T. Park, H.Q. Luo, S. Li, P. Dai, arXiv:1507.04191, 2015.
[50] D.S. Inosov, C. R. Physique 17 (1–2) (2016) 60–89, this issue.
[51] R.M. Fernandes, A.V. Chubukov, J. Schmalian, Nat. Phys. 10 (2014) 97.
[52] T. Goto, R. Kurihara, K. Araki, K. Mitsumoto, M. Akatsu, Y. Nemoto, S. Tatematsu, M. Sato, J. Phys. Soc. Jpn. 80 (2011) 073702.
[53] M. Yoshizawa, D. Kimura, T. Chiba, S. Simayi, Y. Nakanishi, K. Kihou, C.H. Lee, A. Iyo, H. Eisaki, M. Nakajima, S. Uchida, J. Phys. Soc. Jpn. 81 (2012) 024604.
[54] A.E. Bohmer, F. Burger, F. Hardy, T. Wolf, P. Schweiss, R. Fromknecht, M. Reinecker, W. Schranz, C. Meingast, Phys. Rev. Lett. 112 (2014) 047001.
[55] A.E. Böhmer, C. Meingast, C. R. Physique 17 (1–2) (2016) 90–112, this issue.
[56] F.L. Ning, K. Ahilan, T. Imai, A.S. Sefat, M.A. McGuire, B.C. Sales, D. Mandrus, P. Cheng, B. Shen, H.H. Wen, Phys. Rev. Lett. 104 (2010) 037001.
[57] Y. Nakai, T. Iye, S. Kitagawa, K. Ishida, H. Ikeda, S. Kasahara, H. Shishido, T. Shibauchi, Y. Matsuda, T. Terashima, Phys. Rev. Lett. 105 (2010) 107003.
[58] M. Fu, T. Torchetti, T. Imai, F.L. Ning, J.Q. Yan, A.S. Sefat, Phys. Rev. Lett. 109 (2012) 247001.
[59] J. Zhao, D.X. Yao, S. Li, T. Hong, Y. Chen, S. Chang, W. Ratcliff ll, J.W. Lynn, H. Mook, G.F. Chen, J.L. Luo, N.L. Wang, E.W. Carlson, J.P. Hu, P. Dai, Phys. Rev. Lett. 101 (2008) 167203.
[60] R.J. McQueeney, S.O. Diallo, V.P. Antropov, G.D. Samolyu, C. Broholm, N. Ni, S. Nandi, M. Yethiraj, J.L. Zaretsky, J.J. Pulikkotil, A. Kreyssig, M.D. Lumsden, B.N. Harmon, P.C. Canfield, A.I. Goldman, Phys. Rev. Lett. 101 (2008) 227205.
[61] R.A. Ewing, T.G. Perring, R.I. Bewley, T. Guidi, M.J. Pitcher, D.R. Parker, S.J. Clarke, A.T. Boothroyd, Phys. Rev. B 78 (2008) 220501.
[62] J.-H. Chu, H.H. Kuo, J.G. Analytis, I.R. Fisher, Science 337 (2012) 710.
[63] H.H. Kuo, M.C. Shapiro, S.C. Riggs, I.R. Fisher, Phys. Rev. B 88 (2013) 085113.
[64] H.H. Kuo, I.R. Fisher, Phys. Rev. Lett. 112 (2014) 227001.
[65] L. Tassini, F. Venturini, Q.M. Zhang, R. Hackl, N. Kikugawa, T. Fujita, Phys. Rev. Lett. 95 (2005) 117002.
[66] I.J. Pomeranchuk, J. Exp. Theor. Phys. 8 (1958) 361.
[67] E. Bascones, B. Valenzuela, M.J. Calderón, C. R. Physique 17 (1–2) (2016) 36–59, this issue.
[68] M. Zacharias, P. Wölfle, M. Garst, Phys. Rev. B 80 (2009) 165116.
[69] H. Kontani, Y. Yamakawa, Phys. Rev. Lett. 113 (2014) 047001.
[70] M.V. Klein, Electronic Raman Scattering, Topics in Applied Physics, vol. 8, Springer, Berlin, Heidelberg, 1983.
[71] Thomas P. Devereaux, Rudi Hackl, Rev. Mod. Phys. 79 (2007) 175.
[72] N.W. Ashcroft, N.D. Mermin, Solid State Physics, Harcourt, 1976.
[73] H. Yamase, R. Zeyher, Phys. Rev. B 83 (2011) 115116.
[74] H. Yamase, R. Zeyher, Phys. Rev. B 88 (2013) 125120.
[75] Y. Gallais, R.M. Fernandes, I. Paul, L. Chauvière, X.Y. Yang, M.A. Méasson, M. Cazayous, A. Sacuto, D. Colson, A. Forget, Phys. Rev. Lett. 111 (2013) 267001.
[76] A. Cano, M. Civelli, I. Eremin, I. Paul, Phys. Rev. B 82 (2010) 020408.
[77] Mario Zacharias, Indranil Paul, Markus Garst, Phys. Rev. Lett. 115 (Jul 2015) 025703.
[78] M. Daghofer, A. Nicholson, A. Moreo, E. Dagotto, Phys. Rev. B 81 (2010) 014511.
[79] Y. Su, H. Liao, T. Li, J. Phys. Condens. Matter 27 (2015) 105702.
[80] K. Jiang, J.P. Hu, H. Ding, Z. Wang, arXiv:1508.00588, 2015.
[81] M.D. Watson, T.K. Kim, A.A. Haghighirad, N.R. Davies, A. McCollam, A. Narayanan, S.F. Blake, Y.L. Chen, S. Ghannadzadeh, A.J. Schofield, M. Hoesh, C. Meingast, T. Wolf, A.I. Coldea, Phys. Rev. B 91 (2015) 155106.
[82] Weicheng Lv, Jiansheng Wu, Philip Phillips, Phys. Rev. B 80 (2009) 224506.
[83] B. Valenzuela, M.J. Calderón, G. León, L. Bascones, Phys. Rev. B 87 (2013) 075136.
[84] S. Raghu, Xiao-Liang Qi, Chao-Xing Liu, D.J. Scalapino, Shou-Cheng Zhang, Phys. Rev. B 77 (2008) 220503.
[85] Paul C. Canfield, Sergey L. Bud'ko, Annu. Rev. Condens. Matter Phys. 1 (2010) 27.
[86] Marianne Rotter, Marcus Tegel, Dirk Johrendt, Phys. Rev. Lett. 101 (2008) 107006.
[87] Q. Huang, Y. Qiu, Wei Bao, M.A. Green, J.W. Lynn, Y.C. Gasparovic, T. Wu, G. Wu, X.H. Chen, Phys. Rev. Lett. 101 (2008) 257003.
[88] F. Rullier-Albenque, D. Colson, A. Forget, H. Alloul, Phys. Rev. Lett. 103 (2009) 057001.
[89] C. Lester, Jiun-Haw Chu, J. Analytis, S.C. Capelli, A. Erickson, C. Condron, M. Toney, I. Fisher, S. Hayden, Phys. Rev. B 79 (2009) 144523.
[90] D. Pratt, W. Tian, A. Kreyssig, J. Zarestky, S. Nandi, N. Ni, S. Bud'ko, P. Canfield, A. Goldman, R. McQueeney, Phys. Rev. Lett. 103 (2009) 087001.
[91] M.G. Kim, R.M. Fernandes, A. Kreyssig, J.W. Kim, A. Thaler, S.L. Bud'ko, P.C. Canfield, R.J. McQueeney, J. Schmalian, A.I. Goldman, Phys. Rev. B 83 (2011) 134522.
[92] F. Rullier-Albenque, D. Colson, A. Forget, P. Thuery, S. Poissonnet, Phys. Rev. B 81 (2010) 224503.
[93] L. Chauvière, Y. Gallais, M. Cazayous, A. Sacuto, M. Méasson, D. Colson, A. Forget, Phys. Rev. B 80 (2009) 094504.

[94] H.Z. Arham, C.R. Hunt, W.K. Park, J. Gillett, S.D. Das, S.E. Sebastian, Z.J. Xu, J.S. Wen, Z.W. Lin, Q. Li, G. Gu, A. Thaler, S. Ran, S.L. Bud'ko, P.C. Canfield, D.Y. Chung, M.G. Kanatzidis, L.H. Greene, Phys. Rev. B 85 (2012) 214515.
[95] B. Valenzuela, E. Bascones, M.J. Calderón, Phys. Rev. Lett. 105 (2010) 207202.
[96] R.M. Fernandes, E. Abrahams, J. Schmalian, Phys. Rev. Lett. 107 (2011) 217002.
[97] Maxim Breitkreiz, P.M.R. Brydon, Carsten Timm, Phys. Rev. B 90 (2014) 121104.
[98] M.N. Gastiasoro, I. Paul, Y. Wang, P.J. Hirschfeld, B.M. Andersen, Phys. Rev. Lett. 113 (2014) 127001.
[99] Y. Wang, Maria N. Gastiasoro, Brian M. Andersen, M. Tomić, Harald O. Jeschke, Roser Valentí, Indranil Paul, P.J. Hirschfeld, Phys. Rev. Lett. 114 (Mar 2015) 097003.
[100] H.H. Kuo, J.-H. Chu, S.A. Kivelson, I.R. Fisher, arXiv:1503.00402v1, 2015.
[101] A.E. Bohmer, T. Arai, F. Hardy, T. Hattori, T. Iye, H.v. Löhneysen, K. Ishida, C. Meingast, Phys. Rev. Lett. 114 (2015) 027001.
[102] D. Parshall, L. Pintschovius, J.L. Niedziela, J.P. Castellan, D. Lamago, R. Mittal, T. Wolf, D. Reznik, Phys. Rev. B 91 (2015) 134426.
[103] M.P. Allan, T.-M. Chuang, F. Massee, Yang Xie, Ni Ni, S.L. Bud'ko, G.S. Boebinger, Q. Wang, D.S. Dessau, P.C. Canfield, M.S. Golden, J.C. Davis, Nat. Phys. 9 (2013) 220.
[104] E.P. Rosenthal, E.F. Andrade, C.J. Arguello, R.M. Fernandes, L.Y. Xing, X.C. Wang, C.Q. Jin, A.J. Millis, A.N. Pasupathy, Nat. Phys. 10 (2014) 1038.
[105] M.N. Gastiasoro, P.J. Hirschfeld, B.M. Andersen, Phys. Rev. B 89 (2014) 100502.
[106] K. Sugimoto, P. Prelovsek, E. Kaneshita, T. Tohyama, Phys. Rev. B 90 (2014) 125157.
[107] T. Iye, M.-H. Julien, H. Mayaffre, M. Horvatic, C. Berthier, K. Ishida, H. Ikeda, S. Kasahara, T. Shibauchi, Y. Matsuda, T. Terashima, J. Phys. Soc. Jpn. 84 (2015) 043705.
[108] S. Kasahara, H.J. Shi, K. Hashimoto, S. Tonegawa, Y. Mizukami, T. Shibauchi, K. Sugimoto, T. Fukuda, T. Terashima, A.H. Nevidomskyy, Y. Matsuda, Nature 486 (2012) 382.
[109] Y.-X. Yang, Y. Gallais, R.M. Fernandes, I. Paul, L. Chauvière, M.A. Méasson, M. Cazayous, A. Sacuto, D. Colson, A. Forget, JPS Conf. Ser. (2014) 015001.
[110] C. Mirri, A. Dusza, S. Bastelberger, M. Chinotti, L. Degiorgi, J.-H. Chu, H.H. Kuo, I.R. Fisher, Phys. Rev. Lett. 115 (2015) 107001.
[111] S. Liang, A. Moreo, E. Dagotto, Phys. Rev. Lett. 111 (2013) 047004.
[112] I. Paul, Phys. Rev. B 90 (2014) 115102.
[113] H. Yamase, R. Zeyher, New J. Phys. 17 (2015) 073030.
[114] M. Khodas, A. Levchenko, Phys. Rev. B 91 (2015) 235119.
[115] U. Karahasanovic, F. Kretzschmar, T. Böhm, R. Hackl, I. Paul, Y. Gallais, J. Schmalian, Phys. Rev. B 92 (2015) 075134.
[116] F. Kretzschmar, T. Böhm, U. Karahasanovic, B. Muschler, A. Baum, D. Jost, J. Schmalian, S. Caprara, M. Grilli, C. Di Castro, J.G. Analytis, J.-H. Chu, I.R. Fisher, R. Hackl, arXiv:1507.06116, 2015.
[117] R.M. Fernandes, A. Bohmer, C. Meingast, J. Schmalian, Phys. Rev. Lett. 111 (2013) 137001.
[118] K. Nakayama, Y. Miyata, G. Phan, T. Sato, Y. Tanabe, T. Urata, K. Tanigaki, T. Takahashi, Phys. Rev. Lett. 113 (2014) 237001.
[119] S.H. Baek, D.V. Efremov, J.M. Ok, J.S. Kim, J. van den Brink, B. Büchner, Nat. Mater. 14 (2015) 210.
[120] P. Massat, Y. Gallais, M.A. Méasson, M. Cazayous, A. Sacuto, P. Toulemonde, T. Watashige, S. Kasahara, Y. Matsuda, unpublished, 2015.
[121] S. Avci, O. Chmaissem, S. Rosenkranz, J. Allred, I. Eremin, A.V. Chubukov, D.Y. Chung, M.G. Kanatzidis, J.P. Castellan, J.A. Schlueter, H. Claus, D. Khalyavin, P. Manuel, A. Daoud-Aladine, R. Osborn, Nat. Commun. 5 (2014) 3845.
[122] D.D. Khalyavin, S.W. Lovesey, P. Manuel, F. Kruger, S. Rosenkranz, J. Allred, O. Chmaissem, R. Osborn, Phys. Rev. B 90 (2014) 174511.
[123] A.E. Böhmer, F. Hardy, L. Wang, T. Wolf, P. Schweiss, C. Meingast, Nat. Commun. 6 (2015) 7911.
[124] J.M. Allred, K.M. Taddei, D.E. Bugaris, M.J. Krogstad, S.H. Lapidus, D.Y. Chung, H. Claus, M.G. Kanatzidis, D.E. Brown, J. Kang, R.M. Fernandes, I. Eremin, S. Rosenkranz, O. Chmaissem, R. Osborn, arXiv:1505.06175v1, 2015.
[125] J.M. Tranquada, B.J. Sternlieb, J.D. Axe, Y. Nakamura, S. Uchida, Nature 375 (1995) 561.
[126] Y. Ando, K. Segawa, S. Komiya, A.N. Lavrov, Phys. Rev. Lett. 88 (2002) 137005.
[127] R. Daou, J. Chang, D. LeBoeuf, O. Cyr-Choisnière, F. Laliberté, N. Doiron-Leyraud, B. Ramshaw, R. Liang, D.A. Bonn, W.N. Hardy, L. Taillefer, Nature 463 (2010) 519.
[128] M.J. Lawler, K. Fujita, J. Lee, A.R. Schmidt, Y. Kohsaka, C.K. Kim, H. Eisaki, S. Uchida, J.C. Davis, J.P. Sethna, E.A. Kim, Nature 466 (2010) 347.
[129] T. Wu, H. Mayaffre, S. Krämer, M. Horvatič, C. Berthier, W.N. Hardy, R. Liang, D.A. Bonn, M.-H. Julien, Nature 477 (2011) 191.
[130] G. Ghiringhelli, M. Le Tacon, M. Minola, S. Blanco-Canosa, C. Mazzoli, N.B. Brookes, G.M. De Luca, A. Frano, D.G. Hawthorn, F. He, T. Loew, M.M. Sala, D.C. Peets, M. Salluzo, E. Schierle, R. Sutarto, G. Sawatzky, E. Weschke, B. Keimer, L. Braicovich, Science 337 (2012) 821.
[131] J. Chang, E. Blackburn, A.T. Holmes, N. Christensen, J. Larsen, J. Mesot, R. Liang, D.A. Bonn, W.N. Hardy, A. Watenphul, M. v. Zimmermann, E.M. Forgan, S.M. Hayden, Nat. Phys. 8 (2012) 871.
[132] S. Caprara, C. Di Castro, M. Grilli, D. Suppa, Phys. Rev. Lett. 95 (2005) 117004.
[133] L. Tassini, W. Prestel, A. Erb, M. Lambacher, R. Hackl, Phys. Rev. B 78 (2008) 020511.
[134] S. Caprara, M. Colonna, C. Di Castro, R. Hackl, B. Muschler, L. Tassini, M. Grilli, Phys. Rev. B 91 (2015) 205115.
[135] S. Wakimoto, R.J. Birgeneau, M.A. Kastner, Y.S. Lee, R. Erwin, P.M. Gehring, S.H. Lee, M. Fujita, K. Yamada, Y. Endoh, K. Hirota, G. Shirane, Phys. Rev. B 61 (1999) 3699.
[136] S. Caprara, C. Di Castro, B. Mushler, W. Prestel, R. Hackl, M. Lambacher, A. Erb, S. Komiya, Y. Ando, M. Grilli, Phys. Rev. B 84 (2011) 054508.
[137] M. Opel, R. Nemetschek, C. Hoffmann, R. Philipp, P.F. Muller, R. Hackl, I. Tutto, A. Erb, B. Revaz, E. Walker, H. Berger, L. Forro, Phys. Rev. B 61 (2000) 9752.
[138] Y. Gallais, A. Sacuto, T.P. Devereaux, D. Colson, A. Forget, Phys. Rev. B 71 (2005) 012506.
[139] D. LeBoeuf, S. Kramer, W.N. Hardy, R. Liang, D.A. Bonn, C. Proust, Nat. Phys. 9 (2013) 79.
[140] S.E. Sebastian, N. Harrison, F.F. Balakirev, M.M. Altarawneh, P.A. Goddard, R. Liang, D.A. Bonn, W.N. Hardy, G. Lonzarich, Nature 511 (2014) 61.
[141] W. Tabis, Y. Li, M. Le Tacon, L. Braicovich, A. Kreyssig, M. Minola, G. Dellea, E. Weschke, M.J. Veit, M. Ramazanoglu, A.I. Goldman, T. Schmitt, G. Ghiringhelli, N. Barisic, M.K. Chan, C.J. Dorow, G. Yu, X. Zhao, B. Keimer, M. Greven, Nat. Commun. 5 (2014) 5875.
[142] S. Blanco-Canosa, A. Frano, E. Schierle, S. Porras, T. Loew, M. Minola, M. Bluschke, E. Weschke, B. Keimer, M. Le Tacon, Phys. Rev. B 90 (2014) 054513.
[143] M. Hücker, N.B. Christensen, A.T. Holmes, E. Blackburn, E.M. Forgan, R. Liang, D.A. Bonn, W.N. Hardy, O. Gutowski, M. v. Zimmermann, S.M. Hayden, J. Chang, Phys. Rev. B 90 (2014) 054514.
[144] K. Fujita, C.K. Kim, I. Lee, J. Lee, M.H. Hamidian, I.A. Firmo, S. Mukhopadhyay, H. Eisaki, S. Uchida, M.J. Lawler, E.A. Kim, J.C. Davis, Science 344 (2014) 612.
[145] R. Comin, R. Sutarto, E.H. da Silva Neto, L. Chauvière, R. Liang, W.N. Hardy, D.A. Bonn, F. He, G. Sawatzky, A. Damascelli, Science 347 (2015) 1335.
[146] N. Doiron-Leyraud, S. Badoux, S. Rene de Cotret, S. Lepault, D. LeBoeuf, F. Laliberté, E. Hassinger, B. Ramshaw, D.A. Bonn, W.N. Hardy, R. Liang, J.-H. Park, D. Vignolles, B. Vignolle, L. Taillefer, C. Proust, Nat. Commun. 6 (2015) 6034.
[147] E.M. Forgan, E. Blackburn, A.T. Holmes, A. Briffa, J. Chang, L. Bouchenoire, S.D. Brown, R. Liang, D.A. Bonn, W.N. Hardy, N.B. Christensen, M. v. Zimmermann, M. Hücker, S.M. Hayden, arXiv:1504.01585, 2015.
[148] D. Haug, V. Hinkov, Y. Sidis, P. Bourges, N.B. Christensen, A. Ivanov, T. Keller, C.T. Lin, B. Keimer, New J. Phys. 12 (2010) 105006.
[149] Kazuhiko Kuroki, Hidetomo Usui, Seiichiro Onari, Ryotaro Arita, Hideo Aoki, Phys. Rev. B 79 (2009) 224511.

[150] F. Wang, H. Zhai, D.-H. Lee, Europhys. Lett. 85 (2009) 37005.
[151] S. Graser, T.A. Maier, P.J. Hirschfeld, D.J. Scalapino, New J. Phys. 11 (2009) 025016.
[152] S. Graser, A.F. Kemper, T.A. Maier, H.-P. Cheng, P.J. Hirschfeld, D.J. Scalapino, Phys. Rev. B 81 (2010) 214503.
[153] R. Thomale, C. Platt, W. Hanke, J.P. Hu, B.A. Bernevig, Phys. Rev. Lett. 107 (2011) 117001.
[154] S. Maiti, M.M. Korshunov, T.A. Maier, P.J. Hirschfeld, A.V. Chubukov, Phys. Rev. Lett. 107 (2011) 147002.
[155] S. Maiti, M.M. Korshunov, T.A. Maier, P.J. Hirschfeld, A.V. Chubukov, Phys. Rev. B 84 (2011) 224505.
[156] R.M. Fernandes, A.J. Millis, Phys. Rev. Lett. 111 (2013) 127001.
[157] T.A. Maier, D.J. Scalapino, arXiv:1405.5238v1, 2014.
[158] S. Lederer, Y. Schattner, E. Berg, S.A. Kivelson, Phys. Rev. Lett. 114 (2015) 097001.
[159] S. Nandi, M.G. Kim, A. Kreyssig, R.M. Fernandes, D.K. Pratt, A. Thaler, N. Ni, S.L. Bud'ko, P.C. Canfield, J. Schmalian, R.J. McQueeney, A.I. Goldman, Phys. Rev. Lett. 104 (2010) 057006.
[160] E.G. Moon, S. Sachdev, Phys. Rev. B 82 (2010) 104516.
[161] R.M. Fernandes, S. Maiti, P. Wölfle, A.V. Chubukov, Phys. Rev. Lett. 111 (2013) 057001.
[162] Y. Gallais, I. Paul, L. Chauvière, J. Schmalian, arXiv:1504.04570, 2015.
[163] L. Chauvière, Y. Gallais, M. Cazayous, M. Méasson, A. Sacuto, D. Colson, A. Forget, Phys. Rev. B 82 (2010) 180521.
[164] B. Muschler, W. Prestel, R. Hackl, T.P. Devereaux, J.G. Analytis, Jiun-haw Chu, I.R. Fisher, Phys. Rev. B 80 (2009) 180510.
[165] S. Sugai, Y. Mizuno, K. Kiho, M. Nakajima, C. Lee, A. Iyo, H. Eisaki, S. Uchida, Phys. Rev. B 82 (2010) 140504.
[166] I. Mazin, T. Devereaux, J. Analytis, Jiun-Haw Chu, I. Fisher, B. Muschler, R. Hackl, Phys. Rev. B 82 (2010) 180502.
[167] C. Setty, J.P. Hu, Phys. Rev. B 89 (2014) 180509.
[168] K. Terashima, Y. Sekiba, J.H. Bowen, K. Nakayama, T. Kawahara, T. Sato, P. Richard, Y.-M. Xu, L.J. Li, G.H. Cao, Z.-A. Xu, H. Ding, T. Takahashi, Proc. Natl. Acad. Sci. USA 106 (2009) 7330.
[169] T. Hajiri, T. Ito, M. Matsunami, B.H. Min, Y.S. Kwon, S. Kimura, J. Phys. Soc. Jpn. 83 (2014) 093703.
[170] V.K. Thorsmolle, M. Khodas, Z.P. Yin, C. Zhang, S.V. Carr, P. Dai, G. Blumberg, arXiv:1410.6456v1, 2014.
[171] A.V. Chubukov, I. Eremin, M.M. Korshunov, Phys. Rev. B 79 (2009) 220501.
[172] W.C. Lee, S.C. Zhang, C. Wu, Phys. Rev. Lett. 102 (2009) 217002.
[173] D.J. Scalapino, T.P. Devereaux, Phys. Rev. B 90 (2009) 140512.
[174] T.T. Ong, P. Coleman, Phys. Rev. Lett. 111 (2013) 217003.
[175] M. Marciani, L. Fanfarillo, C. Castellani, L. Benfatto, Phys. Rev. B 88 (2013) 214508.
[176] A. Bardasis, J.R. Schrieffer, Phys. Rev. 121 (1961) 1050.
[177] S. Maiti, P.J. Hirschfeld, arXiv:1507.07501, 2015.
[178] F. Kretzschmar, B. Muschler, T. Böhm, A. Baum, R. Hackl, H.H. Wen, V. Tsurkan, J. Deisenhofer, A. Loidl, Phys. Rev. Lett. 110 (2013) 187002.
[179] T. Böhm, A.F. Kemper, B. Moritz, F. Kretzschmar, B. Muschler, H.M. Eiter, R. Hackl, T.P. Devereaux, D.J. Scalapino, H.H. Wen, Phys. Rev. X 4 (2014) 041046.
[180] W.C. Lee, P.W. Phillips, Europhys. Lett. 103 (2013) 57003.
[181] M. Khodas, A.V. Chubukov, G. Blumberg, Phys. Rev. B 89 (2014) 245134.
[182] H. Monien, A. Zawadowski, Phys. Rev. B 41 (1990) 8798.
[183] P. Massat, Y. Gallais, M.A. Méasson, M. Cazayous, A. Sacuto, H.H. Wen, X.H. Chen, unpublished, 2015.
[184] Y. Gallais, in: APS March Meeting, 2015, Y51.00003.
[185] M.C. Rahn, R.A. Ewings, S.J. Sedlmaier, S.J. Clarke, A.T. Boothroyd, Phys. Rev. B 91 (2015) 180501.
[186] Q. Wang, Y. Shen, B. Pan, Y. Hao, M. Ma, F. Zhou, P. Steffens, K. Schmalzl, T.R. Forrest, M. Abdel-Hafiez, D.A. Chaarev, A.N. Vasiliev, P. Bourges, Y. Sidis, H. Cao, J. Zhao, arXiv:1502.07544, 2015.
[187] Y. Lemonik, I.L. Aleiner, C. Toke, V.I. Fal'ko, Phys. Rev. B 82 (2010) 201408.
[188] O. Vafek, K. Yang, Phys. Rev. B 81 (2010) 041401.
[189] A.S. Mayorov, D.C. Elias, M. Mucha-Kruczynski, R.V. Gorbachev, T. Tudoroskiy, A. Zhukov, S.V. Morozov, M.I. Katsnelson, V.I. Fal'ko, A.K. Geim, K.S. Novoselov, Science 333 (2011) 860.
[190] R. Küchler, L. Steinke, R. Daou, M. Brando, K. Behnia, F. Steglich, Nat. Mater. 13 (2014) 461.
[191] A. Collaudin, B. Fauqué, Y. Fuseya, W. Kang, K. Behnia, Phys. Rev. X 5 (2015) 021022.
[192] Y.P. Shkolnikov, S. Misra, N.C. Bishop, E.P. De Poortere, M. Shayegan, Phys. Rev. Lett. 95 (2005) 066809.
[193] O. Gunawan, Y.P. Shkolnikov, K. Vakili, T. Gokmen, E.P. De Poortere, M. Shayegan, Phys. Rev. Lett. 97 (2006) 186404.
[194] C.W. Hicks, D. Brodsky, E.A. Yelland, A.S. Gibbs, J.A.N. Bruin, M.E. Barber, S.D. Edkins, K. Nishimura, S. Yonezawa, Y. Maeno, A.P. Mackenzie, Science 344 (2014) 283.